Turkish Journal of Earth Sciences (Turkish J. Earth Sci.), Vol. 18, 2009, pp. 351–382. Copyright ©TÜBİTAK
doi:10.3906/yer-0705-2 First published online 24 March 2009

Empirical Attenuation Relationships for Western Anatolia, Turkey

NİHAL AKYOL[1] & ÖZLEM KARAGÖZ[2]

[1] Dokuz Eylül University, Engineering Faculty, Department of Geophysical Engineering,
Tınaztepe Campus, Buca, TR–35160 İzmir, Turkey
(E-mail: nihal.akyol@deu.edu.tr)

[2] Çanakkale Onsekiz Mart University, Engineering & Architecture Faculty,
Department of Geophysical Engineering, Terzioğlu Campus, TR–17020 Çanakkale, Turkey

Received 05 May 2007; revised typescript received 04 September 2008; accepted 04 September 2008

Abstract: Seismic hazard studies have become progressively more important for earthquake engineering applications in western Anatolia, which contains one of the world's best examples of a rapidly extending intra-continental tectonic regime. A two-stage regression analysis was applied to peak ground acceleration and 5%-damped spectral acceleration values of 168 recordings from 49 earthquakes in order to develop empirical attenuation relationships which can be used to predict ground motion for western Anatolia. Moment magnitudes for earthquakes range between 4.0 and 6.4 while the hypocentral distances range between 15 and 200 km in our dataset. Site classifications, as one of the predictor variables for the regression analysis, were obtained using horizontal to vertical spectral ratio estimates. These estimates, together with empirical attenuation relationship predictions, have shown that soil amplification is significant in western Anatolia. Attenuation relationship models that are obtained explicitly account for nonlinear sediment effects for deep soil sites in the region. Nonlinear effects of deep soil sites at lower periods are significant at the higher levels of shaking and manifest over-prediction for acceleration values, while they manifest lower prediction values at lower levels of shaking. Both results from the horizontal to vertical ratio method and the regression analysis show that the number of strong motion stations located on the rock sites in the region should be increased and the present site classification of strong motion stations in Turkey should be re-evaluated in detail. When obtained attenuation relation models were compared with the attenuation relationships based on data from tectonically similar regions, the attenuation relations modelled for a specific region could not, in general, be used in engineering applications realized for another region. Our results also indicate that the spectral acceleration model defined in the Turkish Building Code cannot adequately explain magnitude and distance dependencies in western Anatolia.

Key Words: attenuation relationship, horizontal-to-vertical spectral ratio, peak ground acceleration, nonlinear soil behaviour, western Anatolia, Turkey

Türkiye Batı Anadolu Bölgesi için Ampirik Azalım İlişkileri

Özet: Kıta içi gerilme rejiminin en iyi örneklerden biri olan Batı Anadolu'da, mühendislik uygulamaları için gerekli sismik tehlike çalışmalarının önemi gün geçtikçe artmaktadır. Batı Anadolu için, yer hareketi tahminlerinde kullanılabilecek ampirik azalım ilişkilerini geliştirmek amacıyla, toplam 49 depremden elde edilen 168 kayıda ait pik ivme ve %5-sönümlü spektral ivme değerlerinden oluşan bir veri setine, iki aşamalı regresyon analizi uygulanmıştır. Veri setindeki depremlere ait moment büyüklüğü 4.0–6.4 arasında ve odak uzaklığı ise 15–200 km arasında değişmektedir. Regresyon analizinde yer alan zemin sınıflaması parametresine ulaşmak için yatay-düşey spektral oran tahminleri kullanılmıştır. Bu tahminler ve regresyon analizinden elde edilen sonuçlar göstermiştir ki, bölgede sediment dolgu zemin büyütmeleri oldukça belirgindir. Elde edilen azalım ilişkisi modelleri, net bir şekilde, derin sediment dolgu birimler için zeminin doğrusal olmayan davranışını sergilemektedir. Derin sediment dolgu birimlerde küçük periyot değerleri için gözlenen zeminin doğrusal olmayan davranışı, büyük depremler için yüksek ve küçük depremler için ise düşük yer hareketi tahminlerinin yapılabileceğini vurgulamaktadır. Yatay-düşey spektral oran yöntemi ve regresyon analizinden elde edilen sonuçlar göstermiştir ki, bölgede sağlam zemin üzerinde bulunan kuvvetli yer hareketi kayıtçılarının arttırılması ve Türkiye kuvvetli yer hareketi kayıtçıları zemin sınıflamasının, detaylı bir şekilde yeniden

değerlendirilmesi gerekmektedir. Tektonik olarak benzer özelliklere sahip bölgeler için geliştirilen azalım ilişkileri ile elde ettiğimiz sonuçları karşılaştırdığımızda, belirli bir bölge için modellenen azalım ilişkilerinin, başka bir bölge için gerçekleştirilen mühendislik uygulamalarında genel olarak kullanılamayacağını görmekteyiz. Sonuçlar, aynı zamanda, ülkemiz yapı kodlarında tanımlanmakta olan spektral ivme modelinin, Batı Anadolu için büyüklük (magnitude) ve uzaklık bağımlılığını yeterince ifade edemediğini göstermektedir.

Anahtar Sözcükler: azalım ilişkileri, yatay-düşey spektral oran, maksimum ivme, doğrusal olmayan zemin davranışı, batı Anadolu, Türkiye

Introduction

The combination of the drag caused by subduction along the Aegean Arc, the compression from the continental collision in eastern Anatolia (Turkey) and the Caucasus causes the Turkish plate to move westwards (Figure 1) along two strike-slip fault zones (Taymaz *et al.* 1990, 1991, 2004, 2007; Tan & Taymaz 2006), the North Anatolia Fault Zone to the north and the East Anatolia Fault Zone to the south. In this complex tectonic framework, western Anatolia, which is a part of the 'Aegean extensional province' (Taymaz *et al.* 1991), is one of the most seismically active continental regions in the world and much of it has been undergoing ~N–S-directed extensional deformation. Grabens, trending approximately E–W between basin-bounding normal faults (e.g., Bozkurt 2001) and strike-slip faults accommodating the extension (e.g., Zhu *et al.* 2006a) are the most prominent neotectonic features of the region (Figure 2). Besides several different suggestions of timing and origin of the extension in the region (Bozkurt 2001, 2003), three main processes have been proposed to explain the extension in the region: (1) orogenic collapse of thickened crust following suturing of the Neotethys Ocean; (2) back-arc rifting behind a Tethyan subduction zone to the south; and (3) westward tectonic escape of Anatolia towards the Aegean Sea.

Middle Miocene sediments beneath the younger fill at some localities within actively extending grabens in the region (e.g., Koçyiğit *et al.* 1999; Bozkurt 2001, 2003) indicate that, when extension began, some normal faults had cut through pre-existing depocentres (Westaway *et al.* 2004). These areas contain a high degree of fracturing and permeability and because they are closer to the heating source, high thermal conductivity. The region is a good example of a fast intra-continental extensional tectonic regime with a stress rate of 3–4 cm/year. Increasing lithospheric thinning causes increasing geothermal activity in the region and active tectonics have generated seismic activity with destructive earthquakes.

Even though recent attention has focused on possible strong ground motion in the Marmara Sea in Turkey, historical earthquake activity in western Anatolia shows clear evidence for significant destruction during earthquakes along various structures in the region. Activity on the faults is shown by numerous earthquakes (e.g., 1919 Soma, M= 6.9; 1928 Torbalı, M= 6.3; 1933 Gökova, M= 6.8; 1956 Söke-Balat, M= 7.1; 1965 Salihli, M= 5.8; 1969 Demirci, M= 5.9; 1969 Alaşehir, M= 6.5; 1970 Gediz, M= 7.2; 1986 Çubukdağ, M= 5.5; 2003 Urla, M= 5.8; 2003 Buldan, M=5.4). The earthquake swarm in October 2005 (Urla earthquakes) with several hundred earthquakes per month (including three moderate sized events) is one of the latest manifestations of activity in that region. Moderate-sized earthquakes in western Anatolia (Taymaz & Price 1992; Taymaz 1993) might not cause extensive damage compared to a possible large event in the Marmara Sea in Northwestern Turkey. Nevertheless, they are actually the dominant sources of seismic hazard in the region, because of their larger amplitude at longer periods in deep basin structures of the western Anatolia graben system.

Because of the real earthquake threat in western Anatolia, the need for seismic hazard studies has become progressively more important for earthquake engineering applications. A fundamental requirement for these studies is the determination of predictive attenuation relationships for ground motion (Kramer 1996). Attenuation relationships are

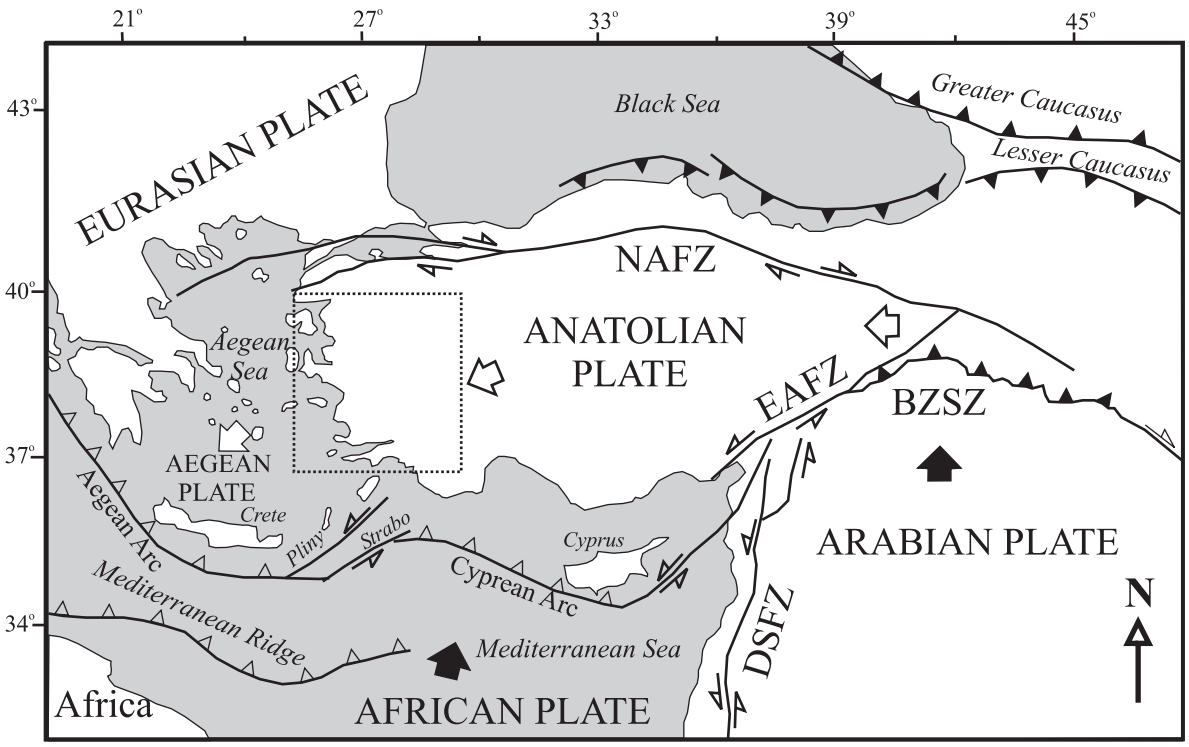

Figure 1. Simplified tectonic map of Turkey showing major neotectonic structures (modified from Taymaz *et al.* 1990, 1991; Barka & Reilinger 1997; Kiratzi & Louvari 2001; Bozkurt & Sözbilir 2004; Akyol *et al.* 2006). DSFZ– Dead Sea Fault Zone, EAFZ– East Anatolia Fault Zone, NAFZ– North Anatolia Fault Zone. Heavy lines with half arrows are strike-slip faults with the arrows showing relative movement sense. Heavy lines with filled triangles show major folds and thrust belts with the triangles indicating the direction of convergence. Heavy lines with open triangles indicate an active subduction zone. Bold filled arrows indicate the movement directions of the African and Arabian plates relative to Eurasia. Open arrows indicate the relative motions of the Anatolia and Aegean plates. The area outlined by dashed lines shows the region of Figure 2.

commonly used to describe how amplitudes of seismic waves decrease with distance, period and earthquake magnitude. Such relationships have been developed for many regions of the world (e.g., Abrahamson & Silva 1997; Gregor *et al.* 2002; Tavaloki & Pezeshk 2005; Bindi *et al.* 2006), mainly by regression of strong-motion data. These studies have shown that the ground motion levels can differ significantly in different tectonic regimes.

Utilizing strong motion data from Turkey, workers have obtained attenuation relationships for several regions. For example, Gülkan & Kalkan (2002) derived empirical attenuation relationships that consider site conditions and fault types, and obtained Peak Ground Acceleration (PGA) and 5%-damped Spectral Acceleration (SA) from a total number of 93 records from 47 horizontal components of 19 events. By using 221 recordings of 122 events, Ulusay *et al.* (2006) generated a PGA attenuation relationship and then prepared an iso-acceleration map of Turkey based on that relationship. Utilizing a database consisting of 195 recordings from 17 events in the Marmara Region, empirical attenuation models for PGA and SA were developed by Özbey *et al.* (2004).

In this study, we have obtained predictive relationships for the ground motion by regressing strong-motion data only from western Anatolia. These relationships will not necessarily apply to other regions of Turkey. We used strong motion records from stations that are located in western Anatolia and operated by the General Directorate of the Disaster Affairs' Earthquake Research Department (ERD) and the data from the WASRE

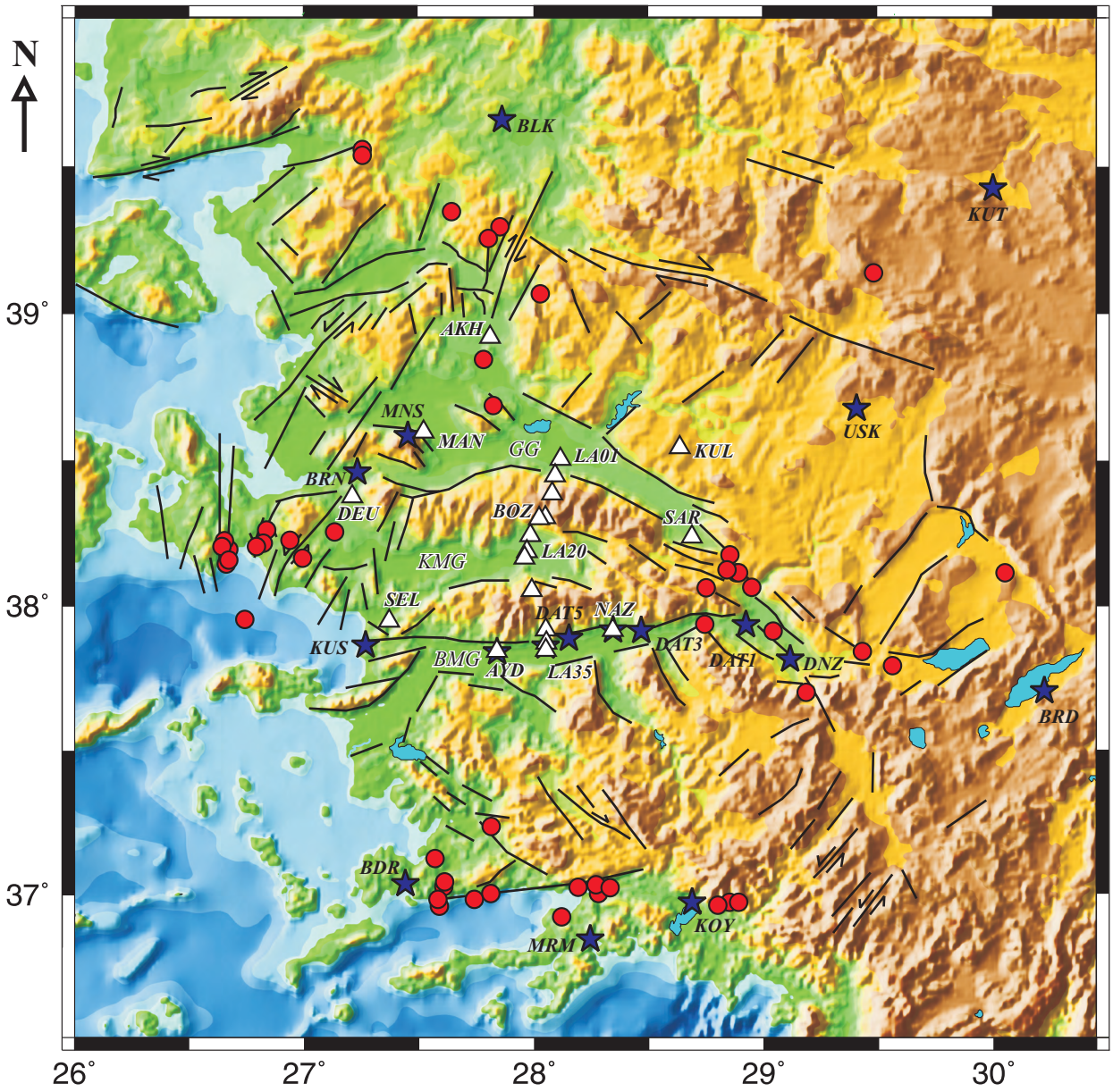

Figure 2. Map showing main tectonic structures in western Anatolia (modified from Akyol *et al.* 2006). The distributions of the events (red circles) and stations (white triangles and dark blue stars represent stations of WASRE and ERD networks, respectively) used in this study. Tectonic features were modified from Şengör *et al.* (1985), Şengör (1987), Konak & Şenel (2002), Şaroğlu *et al.* (1992) and Bozkurt (2000). GG– Gediz Graben, KMG– Küçük Menderes Graben and BMG– Büyük Menderes Graben.

network (Akyol *et al.* 2006). We employed a two-stage regression procedure (e.g., Joyner & Boore 1993; Ambraseys *et al.* 1996; Boore *et al.* 1997) to obtain the PGA and 5%-damped SA attenuation relationships for the region.

Predictor Variables and Data Set

The parameters that must be clearly defined in order to estimate ground motions are earthquake magnitude, distance and local site conditions. Also,

because reverse and thrust earthquakes tend to generate larger peak ground acceleration and high-frequency spectral acceleration than strike-slip and normal earthquakes (Abrahamson & Shedlock 1997), style of faulting should, ideally, be considered when determining ground motion. In this study, however, the style of faulting parameters could not be described, since fault mechanisms are still unknown for most of the events in the region and our dataset is not large enough to distinguish this parameter.

Different definitions for predictor variables in attenuation relationships make them difficult to compare with each other. For example, Ambraseys *et al.* (1996) have generated attenuation relationships using a large data set from European strong motion records. Three different site classes were utilized in their relationship: rock, stiff soil and soft soil. Boore *et al.* (1997) determined a different relationship using strong motion records for shallow earthquakes in western North America. In both models, the distance predictor is r_{jb}, the closest horizontal distance to vertical projection of the rupture (Boore *et al*. 1997). Site condition predictors depend on the average velocities in the upper 30 metres of the crust in the relationship of Boore *et al.* (1997). Sadigh *et al.* (1997) obtained an attenuation relationship for shallow crustal earthquakes based on California strong motion data. They presented relationships for strike-slip and reverse faulting earthquakes, rock and deep firm soil deposits, earthquakes of Mw 4.0 to 8.0 and distances up to 100 km. In their study, the distance predictor is the minimum distance to the rupture surface. Spudich *et al.* (1997) developed their relation based on data from extensional regime earthquakes having $M_w \geq 5.0$ everywhere in the world and that are recorded at distances less than 105 km. They presented relations for horizontal peak acceleration and 5%-damped pseudo-velocity response spectra. The Özbey e*t al.* (2004) attenuation relationship was obtained from 195 strong motion records of 17 earthquakes with $M_w \geq 5.0$. Their data set includes mainly the last largest events in the Marmara Region, the Kocaeli (M_w= 7.4), the Düzce (M_w= 7.1) events and their aftershocks. Their predictors and equation forms are the same as Boore *et al.* (1997). In this study, the predictor variables are described in the following paragraphs.

Local Site Condition Parameter

Most of the data used in this study was obtained from the Turkish National Strong Motion Network (hereafter referred as TNSMN). The data from 18 stations of that network was used (Table 1). Additionally, we used data from the temporary WASRE (Western Anatolia Seismic Recording Experiment [Akyol *et al.* 2006; Zhu *et al.* 2006b]) network that operated between 2002 and 2003 in the region (Table 1). Technical characteristics of the instruments operated by the TNSMN and the WASRE networks were obtained from the internet site of the General Directorate of Disaster Affairs Earthquake Research Department (ERD) of Turkey (http://deprem.gov.tr) and Akyol *et al*. (2006), respectively. One of the main problems is to get detailed information about the Turkish network from which the seismological data have been retrieved. For example, the classifications of TNSMN sites were described in three different classes by ERD, mostly from the properties of surface materials of the sites. Thus, it was decided to classify the records for site conditions according to the frequency band of the fundamental frequency and amplification factor based on Horizontal to Vertical Spectral Ratio (HVSR) estimates for all stations, since there is no more detailed information about strong motion sites in Turkey.

To apply the HVSR method, the initial time of the SH-wave window, which covers the S-wave portion on the seismograms, was selected visually. Only data with S/N ratio greater than three were used to compute the spectral ratios and the spectra were smoothed using a nine-point moving average operator. The HVSR method is based on the so-called Receiver-Function technique applied to studies of the upper mantle and crust using teleseismic records. This method assumes that local site conditions are relatively transparent to the motion that appears on the vertical component. The HVSR method is able to identify resonant frequencies, although the general tendency of the method to underestimate the amplification value has been shown by different workers (e.g., Lachet *et al.* 1996; Theodulidis *et al.* 1996; Akyol *et al*. 2002).

Figure 3 shows individual HVSR results of each event and average site amplifications for MAN and

Table 1. Data used in the development of the attenuation relationships for western Anatolia.

Event No	Data No	Date	Time	Latitude (N)	Longitude (E)	Site	Depth (km)	Original M	Mw	Pga (g)
1	1	06.12.1985	22:35:29.9	36.97	28.85	KOY	9	4.6 mb *(GS)*	4.81	0.11335
2	2	06.11.1992	19:08:09.2	38.16	26.99	KUS	17	6.1 Mw *(GS)*	6.10	0.08461
3	3	13.11.1994	06:56:00.3	36.97	28.89	KOY	7	5.4 Mw *(HRV)*	5.40	0.09585
4	4	13.11.1994	07:58:16	36.96	28.8	KOY	31	4.8 mb *(GS)*	5.06	0.05833
5	5	18.08.1995	00:52:23.8	37.84	29.43	DNZ	6	4.8 mb *(GS)*	5.06	0.01632
6	6	01.10.1995	15:57:13.1	38.11	30.05	BRD	5	6.4 Mw *(HRV)*	6.40	0.03940
	7	01.10.1995	15:57:13.1	38.11	30.05	DNZ	5			0.01632
7	8	20.02.1996	02:53:05.8	38.25	27.13	KUS	31	4.7 Mw *(a)*	4.70	0.02139
8	9	25.02.1998	06:58:01.5	37.79	29.56	DNZ	10	4.4 mb *(GS)*	4.56	0.00460
	10					BRD	10			0.00277
9	11	05.03.1998	01:45:08.9	39.55	27.25	BLK	7	4.9 Mw *(b)*	4.90	0.00634
	12					BRN	7			0.00330
10	13	05.03.1998	01:55:26.7	39.53	27.25	BLK	5	4.4 mb *(GS)*	4.56	0.00978
	14					BRN	5			0.00184
11	15	09.07.1998	17:36:47.8	37.95	26.74	BRN	21	5.6 Mw *(b)*	5.60	0.02758
	16					MNS	21			0.00503
12	17	25.07.1999	06:57:01	39.29	27.85	BLK	10	5.2 Mw *(HRV)*	5.20	0.01469
	18					AYD	10			0.00280
13	19	08.09.2000	05:46:47.3	39.34	27.64	BLK	14	4.6 md *(ERD)*	4.79	0.01033
	20					BRN	14			0.00159
14	21	04.10.2000	02:33:57	37.91	29.04	DNZ	8.4	4.7 md *(ERD)*	4.88	0.06776
	22					USK	8.4			0.00196
15	23	22.06.2001	11:54:51.16	39.25	27.8	BLK	5	5.0 md *(ERD)*	5.17	0.01198
	24					KUT	5			0.00190
16	25	21.01.2002	14:34:24	38.6823	27.8218	BRN	10.1	4.7 md *(ERD)*	4.88	0.00716
17	26	30.07.2002	12:20:23	37.6977	29.1835	DNZ	8.5	4.5 md *(ERD)*	4.69	0.01721
18	27	10.04.2003	00:40:16	38.2568	26.8345	BDR	15.8	5.8 Mw *(c)*	5.80	0.00237
	28					BLK	15.8			0.00352
	29					BRN	15.8			0.08014
	30					DAT01	15.8			0.00481
	31					DAT04	15.8			0.01121
	32					DAT05	15.8			0.00860
	33					DAT06	15.8			0.00790
	34					AYD*	15.8			0.01384
	35					KUL*	15.8			0.01481
	36					LA04*	15.8			0.03130
	37					LA07*	15.8			0.01867
	38					LA13*	15.8			0.01577
	39					LA20*	15.8			0.02617
	40					MAN*	15.8			0.01102
	41					NAZ*	15.8			0.01229
	42					SAR*	15.8			0.00773

Table 1 (Continued)

Event No	Data No	Date	Time	Latitude (N)	Longitude (E)	Site	Depth (km)	Original M	Mw	Pga (g)
19	43	10.04.2003	00:53:48	38.2123	26.8193	BRN	11.4	4.3 Mw *(c)*	4.30	0.00167
	44					DEU*	11.4			0.00286
	45					SEL*	11.4			0.00221
20	46	17.04.2003	22:34:26	38.2223	26.9363	BRN	15.2	5.2 Mw *(c)*	5.20	0.00906
	47					DAT05	15.2			0.00197
	48					AKH*	15.2			0.00442
	49					AYD*	15.2			0.00225
	50					BOZ*	15.2			0.00541
	51					DEU*	15.2			0.01325
	52					KUL*	15.2			0.00307
	53					LA01*	15.2			0.01037
	54					LA04*	15.2			0.00817
	55					LA07*	15.2			0.00720
	56					LA13*	15.2			0.00474
	57					LA16*	15.2			0.00701
	58					LA20*	15.2			0.00574
	59					MAN*	15.2			0.00288
	60					NAZ*	15.2			0.00221
	61					SEL*	15.2			0.01191
21	62	22.06.2003	23:46:20	39.0615	28.0272	BRN	8.9	4.4 Mw *(c)*	4.40	0.00181
	63					LA01*	8.9			0.00747
	64					LA21*	8.9			0.00268
22	65	02.07.2003	01:43:35	38.0602	28.9485	DNZ	5	4.0 md *(ERD)*	4.22	0.00250
23	66	23.07.2003	04:56:02	38.1718	28.8533	DAT04	5	5.4 Mw *(c)*	5.40	0.02646
	67					DNZ	5			0.04675
	68					DAT06	5			0.00851
	69					USK	5			0.00542
	70					BRN	5			0.00227
	71					DAT01	5			0.12568
	72					DAT03	5			0.02216
	73					AYD*	5			0.00750
	74					LA21*	5			0.01241
	75					SAR*	5			0.05179
	76					SEL*	5			0.00415
24	77	26.07.2003	01:00:56	38.11	28.88	DAT01	5	4.9 Mw *(c)*	4.90	0.04849
	78					DAT03	5			0.01147
	79					DAT04	5			0.01716
	80					DAT06	5			0.00342
	81					DNZ	5			0.00630
	82					USK	5			0.00318
	83					AYD*	5			0.00259
	84					BOZ*	5			0.00259

Table 1 (Continued)

Event No	Data No	Date	Time	Latitude (N)	Longitude (E)	Site	Depth (km)	Original M	Mw	Pga (g)
	85					LA21*	5			0.00269
	86					LA26*	5			0.00238
	87					LA34*	5			0.00566
	88					LA35*	5			0.00255
	89					SAR*	5			0.02536
25	90	26.07.2003	08:36:49	38.11	28.89	DAT03	4.3	5.3 Mw *(c)*	5.30	0.02681
	91					DAT04	4.3			0.02770
	92					DAT01	4.3			0.12352
	93					DAT06	4.3			0.00865
	94					DNZ	4.3			0.02630
	95					USK	4.3			0.00668
	96					AYD*	4.3			0.00642
	97					BOZ*	4.3			0.00432
	98					LA21*	4.3			0.00966
	99					LA26*	4.3			0.00865
	100					LA34*	4.3			0.01421
	101					LA35*	4.3			0.00704
	102					SAR*	4.3			0.11707
	103					SEL*	4.3			0.00327
26	104	26.07.2003	13:31:36	38.12	28.84	DAT03	8.5	5.1 Mw *(c)*	5.10	0.01277
	105					DAT04	8.5			0.01877
	106					DAT06	8.5			0.00265
	107					AYD*	8.5			0.00361
	108					LA21*	8.5			0.00278
	109					LA26*	8.5			0.00307
	110					LA32*	8.5			0.00208
	111					SAR*	8.5			0.00941
27	112	12.08.2003	08:21:50	38.059	28.75	DAT01	5	4.5 Mw *(c)*	4.50	0.00716
	113					DAT03	5			0.00422
	114					DAT04	5			0.00471
	115					NAZ*	5			0.00477
	116					SAR*	5			0.00865
28	117	17.04.2004	03:38:40	39.1335	29.4788	KUT	8.5	4.1 ml *(ERD)*	4.78	0.00230
	118					USK	8.5			0.00468
29	119	03.08.2004	05:33:38	37.1222	27.5685	BDR	12.3	4.3 md *(ERD)*	4.50	0.00639
30	120	03.08.2004	13:11:31	36.956	27.5877	BDR	7.6	5.2 Mw *(HRV)*	5.20	0.01612
31	121	04.08.2004	03:01:07	37.0238	27.6063	BDR	15.7	5.6 Mw *(HRV)*	5.60	0.02792
	122					DAT01	15.7			0.00328
	123					DAT05	15.7			0.00241
32	124	04.08.2004	04:19:47	36.98	27.58	DAT04	8	5.0 ml *(ERD)*	5.40	0.00517
	125					DAT05	8			0.00224
	126					DAT06	8			0.00242

Table 1 (Continued)

Event No	Data No	Date	Time	Latitude (N)	Longitude (E)	Site	Depth (km)	Original M	Mw	Pga (g)
33	127	04.08.2004	05:46:15	37.233	27.8133	BDR	5.6	4.2 ml *(ERD)*	4.85	0.00617
34	128	04.08.2004	14:18:48	37.04	27.61	BDR	5	5.3 Mw *(HRV)*	5.30	0.02867
35	129	20.12.2004	23:02:15	37	28.28	BDR	12.5	5.4 Mw *(HRV)*	5.40	0.00775
	130					BRN	12.5			0.00218
	131					DAT01	12.5			0.00782
	132					DAT05	12.5			0.00360
	133					DAT06	12.5			0.00339
	134					KOY	12.5			0.02794
	135					MRM	12.5			0.03890
36	136	28.12.2004	20:34:11	37.03	28.27	MRM	13.9	3.9 md *(ERD)*	4.12	0.00619
37	137	10.01.2005	23:48:51	37	27.81	BDR	15.8	5.5 Mw *(HRV)*	5.50	0.00797
	138					MRM	15.8			0.01721
38	139	11.01.2005	04:35:58	36.98	27.74	BDR	14.9	4.3 md *(ERD)*	4.50	0.01743
	140					KOY	14.9			0.00205
39	141	14.01.2005	19:08:11	37.02	28.33	KOY	15	3.8 md *(ERD)*	4.03	0.00212
	142					MRM	15			0.00290
40	143	29.01.2005	18:52:30	38.2	26.79	BRN	20	4.3 md *(ERD)*	4.50	0.00626
41	144	17.10.2005	05:45:18	38.19	26.67	BRN	20.5	5.0 md *(ERD)*	5.17	0.01684
	145					BLK	20.5			0.00177
42	146	17.10.2005	08:34:44	38.14	26.66	BRN	2.7	4.0 md *(ERD)*	4.22	0.00254
43	147	17.10.2005	09:46:56	38.22	26.65	BLK	18.6	5.8 Mw *(GS)*	5.80	0.00302
	148					BRN	18.6			0.02293
	149					DAT04	18.6			0.00460
	150					DAT06	18.6			0.00310
	151					MNS	18.6			0.00936
44	152	17.10.2005	09:55:31	38.2	26.64	BRN	11	5.2 Mw *(HRV)*	5.20	0.01340
	153					MNS	11			0.01122
45	154	20.10.2005	21:40:02	38.15	26.67	BLK	15.4	5.9 md *(ERD)*	6.02	0.00461
	155					BRN	3.7			0.03256
	156					DAT01	15.4			0.00375
	157					DAT04	15.4			0.00621
	158					DAT06	15.4			0.00421
	159					MNS	15.4			0.02242
46	160	24.12.2005	03:56:07	38.84	27.78	DAT04	6	4.5 ml *(ERD)*	5.10	0.00387
	161					DAT05	6			0.00396
	162					DAT06	6			0.00315
47	163	17.04.2006	11:53:22.27	37.0225	28.191	MRM	11	4.2 md *(ERD)*	4.41	0.01048
48	164	17.04.2006	20:18:07.95	36.9178	28.1197	MRM	31.8	4.0 md *(ERD)*	4.22	0.00743
49	165	05.06.2006	04:23:30.99	37.933	28.743	DAT01	11.1	4.8 Mw *(HRV)*	4.80	0.02330
	166		04:23:30.99			DAT03	11.1			0.06812
	167		04:23:30.99			DAT04	11.1			0.02130
	168		04:23:30.99			DAT05	11.1			0.00586

* represents WASRE stations used in this study. GS, HRV, ATH magnitudes were reported by NEIC. ERD denotes the General Directorate of Disaster Affairs' Earthquake Research Department. (a), (b) and (c) represents magnitude values from Ulusay *et al.* (2004), Zare & Bard (2002) and WASRE network database (Zhu *et al.* 2006a), respectively.

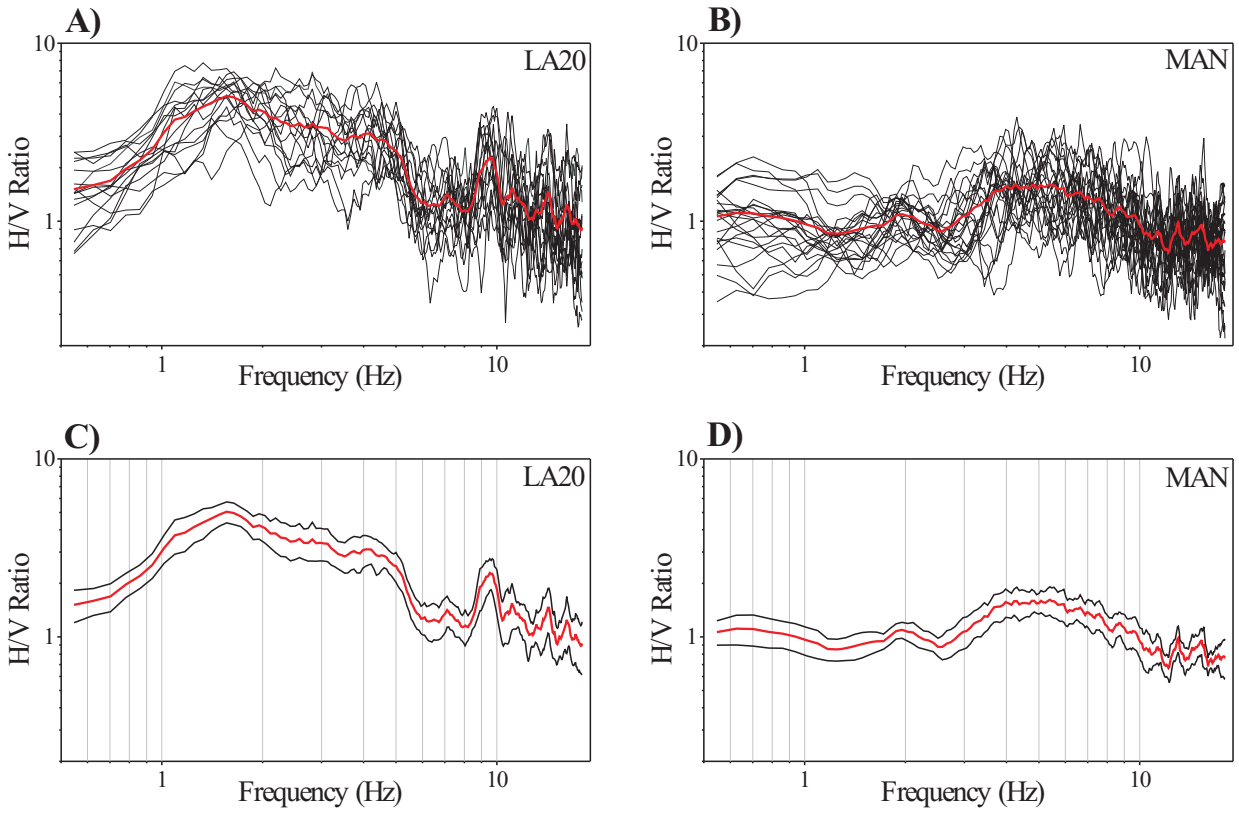

Figure 3. Amplification from all individual events (black lines) for **(a)** LA20 and **(b)** MAN stations from HVSR method. The mean site amplifications for **(c)** LA20 and **(d)** MAN sites (red lines) with 90% confidence intervals (black lines).

LA20 stations. In brief, there are four site categories: Sites 1, 2, 3 and 4 correspond to rock, stiff soil, soil and deep soil sites, respectively (Figure 4). The code, coordinates, site classifications and number of the data used for HVSR estimates and regression analysis for each station are given in Table 2. Since the quality of data is insufficient for obtaining the site parameters for the four different site classes, data from sites 1 and 2 were combined and designated as data from site A. Similarly, data from sites 3 and 4 were combined and designated as data from site B (Figure 5) in the regression analysis.

Distance Parameter

Different source-to-site distance measures have been used by different workers to predict empirical attenuation relationships. These distance measures include r_{jb}, the closest horizontal distance to vertical projection of the rupture (e.g., Boore *et al.* 1997; Gülkan & Kalkan 2002), r_{rup}, the closest distance to the rupture surface (e.g., Abrahamson & Silva 1997; Sadigh *et al.* 1997), r_{seis}, the closest distance to the seismogenic rupture surface (e.g., Campell 1997), and r_{hypo}, the hypocentral distance (e.g., Atkinson & Boore 1997). Atkinson & Boore (1997) had used r_{hypo} for the data generated stochastically by using a Brune point source model characterized by stress parameter of 50 bars. Zare & Bard (2002) prepared a strong motion dataset for all of Turkey and their estimate for the hypocentral distance is mainly based on the well-known formula, $r_{hypo}= 8(t_s-t_p)$, in which t_p and t_s are the first arrivals of P and S wave, respectively.

Since fault geometries are still unknown for most moderate-sized events in the region, r_{hypo} was

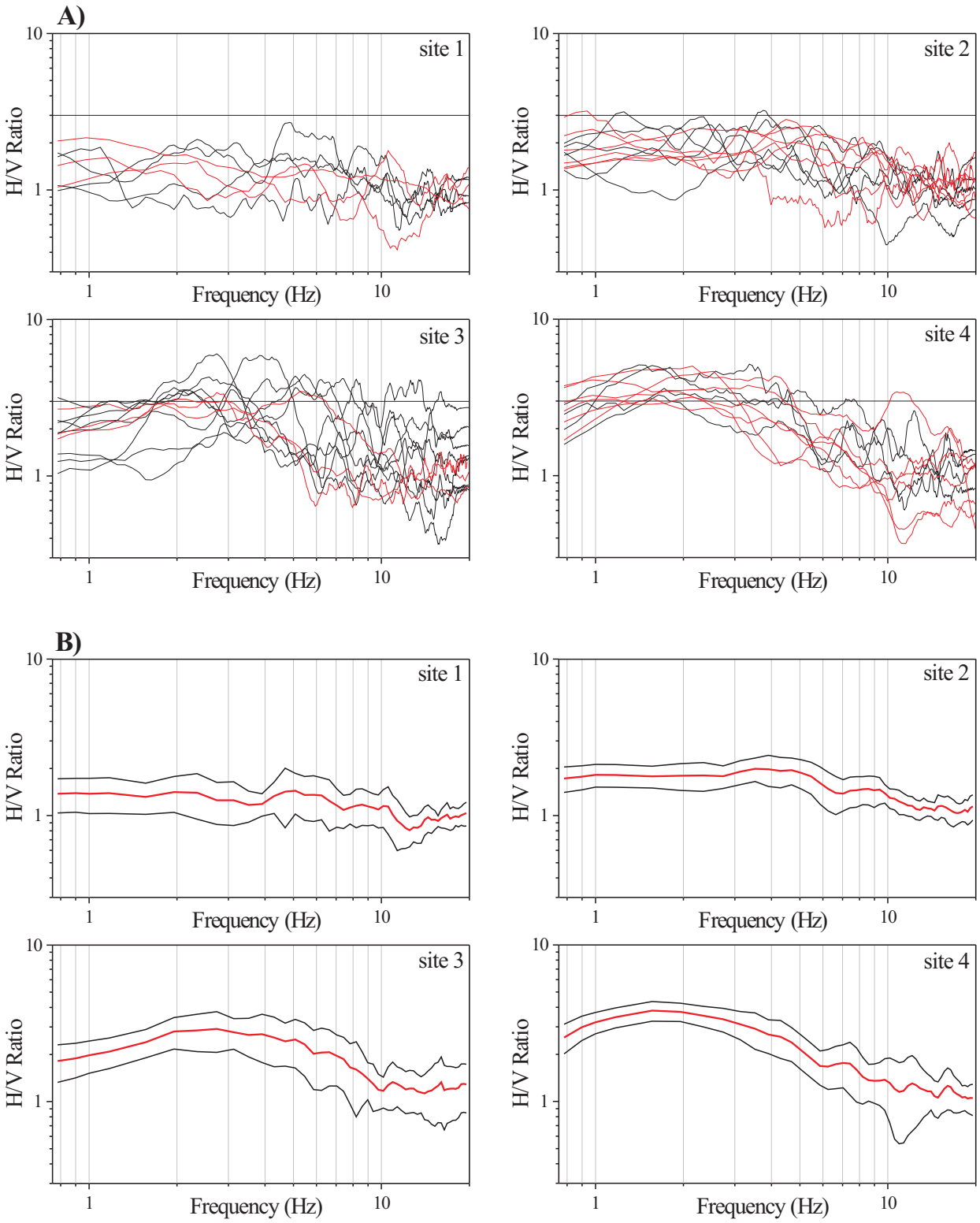

Figure 4. **(a)** The mean site amplifications from HVSR estimates for all stations in site classes 1, 2, 3 and 4. Red and black lines represent ERD and WASRE stations, respectively; **(b)** the mean site amplifications (red lines) for four different site classes with 90% confidence intervals (black lines).

Table 2. Stations with records used in this study.

No	Station Code	Station Latitude (N)	Station Longtitude (E)	N1	N2	Site Class (ERD)	Site Class (in this stuy)
1	AKH*	38.915	27.808	18	1	-	3
2	AYD	37.837	27.838	19	1	S	3
3	AYD*	37.841	27.837	14	6	-	3
4	BDR	37.033	27.440	65	9	H	2
5	BLK	39.650	27.860	44	9	R	2
6	BOZ*	38.300	28.049	14	3	-	3
7	BRD	37.704	30.221	10	2	H	1
8	BRN	38.455	27.229	47	17	S	4
9	DAT1	37.932	28.923	49	9	S	4
10	DAT3	37.912	28.465	11	6	S	3
11	DAT4	37.913	28.343	6	11	S	4
12	DAT5	37.884	28.151	2	7	S	2
13	DAT6	37.857	28.050	6	10	S	2
14	DEU*	38.371	27.208	46	2	-	2
15	DNZ	37.813	29.114	174	9	S	1
16	KOY	36.970	28.687	20	6	S	2
17	KUL*	38.540	28.634	16	2	-	3
18	KUS	37.861	27.266	8	2	S	3
19	KUT	39.419	29.997	3	2	S	2
20	la01*	38.499	28.113	20	2	-	4
21	la04*	38.443	28.091	12	2	-	3
22	la07*	38.381	28.079	29	2	-	3
23	la13*	38.296	28.021	24	2	-	1
24	la16*	38.239	27.983	22	1	-	1
25	la20*	38.184	27.969	16	2	-	4
26	la21*	38.162	27.957	8	5	-	3
27	la26*	38.049	27.989	47	3	-	2
28	la32*	37.915	28.051	7	1	-	2
29	la34*	37.869	28.052	28	2	-	2
30	la35*	37.844	28.051	11	2	-	3
31	MAN*	38.593	27.518	23	2	-	1
32	MNS	38.580	27.450	4	4	S	1
33	MRM	36.840	28.245	17	6	S	4
34	NAZ*	37.913	28.343	5	3	-	4
35	SAR*	38.234	28.686	30	6	-	2
36	SEL*	37.944	27.368	35	4	-	4
37	USK	38.672	29.404	8	5		4

*: WASRE network (Akyol *et al.* 2006) stations. N1 and N2 are total data number using for HVSR estimates and the regression analysis, respectively. According to ERD site classification R– rock, H– stiff soil and, S– soil sites. Site classes 1, 2, 3 and 4 represent rock, stiff soil, soil and deep soil sites.

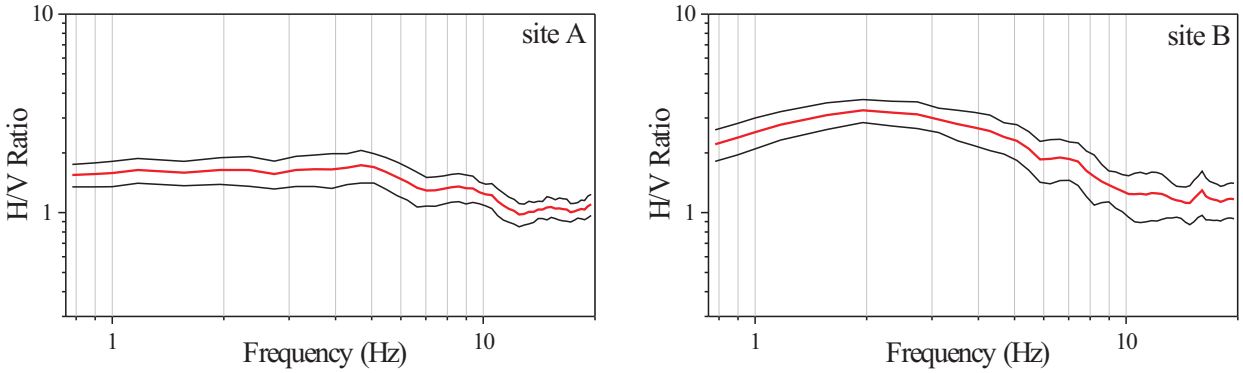

Figure 5. The mean site amplifications (red lines) for site A and B with 90% confidence level (black lines). Data from sites 1 and 2 were combined and designated as data from site A. Similarly, data from sites 3 and 4 were combined and designated as data from site B in the regression analysis.

choosen as the predictor variable for distance. In many cases, it has been suggested that using epicentral distance would not cause significant bias because the dimensions of the rupture area for small earthquakes are usually much smaller than the distance to the recording stations (e.g., Ambraseys *et al.* 1996; Gülkan & Kalkan 2002). We believe that using epicentral distance increases distance uncertainties, since most of the events in the region were located by constraining the depth parameters. Thus, good crustal velocity structure (see Saunders *et al.* 1998 for a case study) and well-distributed stations are needed for better location processes. Recently, Zhu *et al.* (2006a) and Akyol *et al.* (2006) have shown that uncertainties of the location result from poor event locations in the catalogues and their lack of correlations with known faults in the region.

Magnitude Parameter

Moment magnitude (M_W) is the preferred magnitude measure to predict empirical attenuation relationships because it is directly related to the seismic moment of the earthquake. However, the magnitude scale of the data from General Directorate of Disaster Affairs' Earthquake Research Department (ERD) includes mostly M_L or M_d values. To homogenize our dataset, we used M_W values reported by NEIC, Ulusay *et al.* (2004), Zare & Bard (2002) and the WASRE network database (Zhu *et al.* 2006a). We have converted original magnitudes, where given in other scales, to M_W using the empirical relationships by Ulusay *et al.* (2004). In that study, based on a database of 170 events in Turkey, the values of M_W (from ETHZ and Harvard) to M_S (from ETHZ, ISC, USGS, Harvard and ISESD), M_b (from ETHZ, ISC, USGS and Harvard), M_d and M_L (from ERD) were correlated. We used their M_W-M_d and M_W-M_L relations:

$$M_w = 0.9495\, M_d + 0.4181 \quad (r=0.94,\ SD=0.716) \qquad (1)$$

$$M_w = 0.7768\, M_L + 1.5921 \quad (r=0.94,\ SD=0.709) \qquad (2)$$

Data Selection Criteria and Processing

We first analyzed a total of 2123 acceleration records from all regions of Turkey. Recordings with unknown and poor estimates of magnitude, distance and/or site conditions were discarded. The final data set consists of 168 horizontal components from 49 events, after applying some restrictions such as the need to lie within certain boundaries (Figure 2), placing an upper limit on distance (r_{hypo} < 200 km), and lower limits on magnitude (Mw ≥ 4.0) and PGA values (PGA > 0.0015 g). Low- and high-frequency noise was checked for all the records. Much data from SMA-1 recorders have significant levels of long period noise (especially for events with low magnitudes or the records with large distances). No

filtering was applied to the data but all suspect data were eliminated. In order to make the records uniform we (1) applied an instrument response correction to all data, (2) numerically differentiated the WASRE network velocity data to obtain acceleration values, and (3) corrected the base line for all data.

Table 1 lists the events, used in this study, with location parameters, sites, original/converted magnitude values and PGA values. The PGA values presented in this table are the largest peak between the two horizontal components. To make the data sets uniform from two different networks, we used location parameters reported by ERD, given in Table 1. Location parameters and magnitude values of the events reported in the WASRE network database (Akyol *et al*. 2006; Zhu *et al*. 2006a) and magnitude values given by ERD for the same events are given in Table 3, in order to compare the results. Distributions of the earthquakes in terms of hypocentral distance, moment magnitude and site conditions are given in Figure 6.

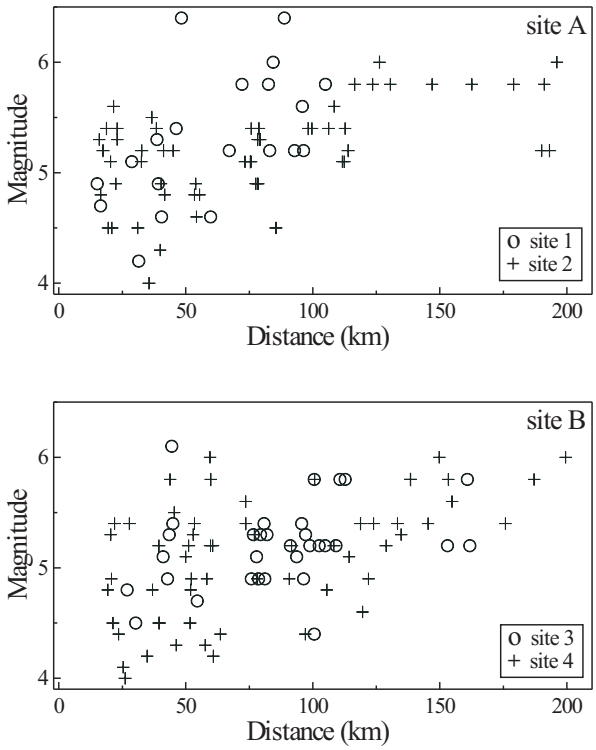

Figure 6. Distribution of the data for **(a)** site A and **(b)** site B in terms of distance and moment magnitude.

Method

The general form of attenuation relationships can be written as follows:

$$\log y_{i,j} = \sum_{i=1}^{N} \sum_{j=1}^{M} (A_i E_i + b_1 r_{i,j} + b_2 \log r_{i,j} + cS_{i,j}) + \varepsilon \quad (3)$$

where,

A_i = specific amplitude factors for each earthquake,

E_i = 1 for earthquake i and 0 otherwise,

N = earthquake number,

Table 3. The location parameters and magnitude values of the events reported by the WASRE network database and magnitude values given by ERD.

Event No	Date	Time	Latitude (N)	Longitude (E)	Depth	Magnitude (ERD)*	Mw
18	11.04.2003	00:40:16.21	38.1987	26.7478	5.90	5.6 md	5.8
19	11.04.2003	00:53:49.22	38.2066	26.8127	5.00	4.2 md	4.3
20	18.04.2003	22:34:24.67	38.2224	26.7556	5.00	4.8 md	5.2
21	23.06.2003	23:46:21.2	39.0301	28.0413	7.94	4.6 md	4.4
23	24.07.2003	04:56:04.48	38.0979	28.8748	8.49	5.2 ml	5.4
24	27.07.2003	01:00:57.73	38.0846	28.9018	9.30	5.0 ml	4.9
25	27.07.2003	08:36:50.34	38.0753	28.909	9.01	5.6 ml	5.3
26	27.07.2003	13:31:36.27	38.1334	28.8637	9.90	4.9 ml	5.1
27	13.08.2003	08:21:50	38.1354	28.8506	8.77	4.3 ml	4.5

* magnitude values reported by ERD.

M = record number for each earthquake,

b_1 = coefficient for anelastic attenuation,

b_2 = coefficient for geometrical spreading,

c = coefficient for site dependence,

S = site classification (here, 0 for site A and 1 for site B),

$r = (d^2+h^2)^{1/2}$ (here, hypocentral distance),

d = epicentral distance,

h = focal depth,

y is the ground motion parameter (e.g., PGA or SA) and $\varepsilon = \sigma P \cdot \sigma$, is the standard deviation of the residuals. The value of P is based on the assumption that the prediction errors are normally distributed and P= 0.84 confidence level for $\pm 1\sigma$ values.

In the recent attenuation relationships, the depth coefficient, h, is estimated as part of the regression and referred as a 'fictitious' depth measure (Boore *et al.* 1997). Abrahamson & Silva (1997) reported that estimated h yielded a marginally better fit to the data at short distances since h incorporated factors that tend to enhance the motion near the source, especially, directivity. To estimate h properly, very close distances between the sources and stations are needed. Since our dataset lacks records with epicentral distance less than 10 km, we could not add the h value as an unknown parameter in the regression.

The coefficients in equation 3 are determined using a two-stage regression procedure (e.g., Ambraseys *et al.* 1996; Boore *et al.* 1997). The distance and site condition dependence, along with a set of amplitude factors, one for each earthquake, were determined in the first stage. In the second stage, the amplitude factors were regressed against magnitude to determine magnitude dependence. Therefore, the data was divided into classes with the two-stage regression analysis, which is a well-known technique (e.g., Draper & Smith 1966; Weisberg 1980). The procedure decouples the determination of magnitude dependence from the determination of distance dependence. If the regression analysis was carried out in terms of magnitude and distance simultaneously, errors in measuring magnitude would affect the distance coefficients obtained from the regression. In this approach, each earthquake has the same weight in determining magnitude dependence and each recording has the same weight in determining distance dependence (Joyner & Boore 1981).

After A_i values are obtained by the first stage, they were used to find, by least squares, a first- or second-order polynomial representing the magnitude dependence.

$$A_i = a_1 + a_2 (M_i - 6) + a_3 (M_i - 6)^2 \quad (4)$$

Here, M is moment magnitude and a_1, a_2 and a_3 are the coefficients determined by the second regression stage. Assuming that arbitrary magnitude and distance parameters do not correlate with each other, we can use the covariance theorem to estimate the total standard error, σ, after two regression stages, using the equation;

$$\sigma = (\sigma_1^2 + \sigma_2^2)½ \quad (5)$$

where, σ_1 is the standard deviation of the residuals from the first regression stage and σ_2 is the standard deviation of the residuals from the second regression stage.

Researchers have used many different forms of this relation. For example, Joyner & Boore (1981) used equation 3, without the b_2 coefficient. In this case, the form chosen for the regression is equivalent to:

$$y = \frac{k}{r} e^{-qr} \quad (6)$$

where k is a function of M and q is a constant. This corresponds to simple point source geometric spreading with constant-Q anelastic attenuation. This form would in fact apply only to a harmonic component of ground motion, not to peak acceleration. However, Joyner and Boore (1981) suggested that its application to peak parameters is an appropriate approximation since coefficients are determined empirically.

Ambraseys *et al.* (1996) used equation 3 and applied a third regression stage to residuals to distinguish different site condition coefficients. Their equation form includes both an anelastic attenuation coefficient (b_1) and geometrical

spreading coefficient (b_2) for distance dependence. However, they accepted values of b_1 equal to zero since they obtained positive b_1 values, while generating strong-motion attenuation relationship for Europe. The anelastic attenuation coefficient, b_1, is also equal to zero attenuation relationship for earthquake ground motions in extensional tectonic regimes in Spudich *et al.* (1997).

Boore *et al.* (1997), Gülkan & Kalkan (2002) and Özbey *et al.* (2004) used only b_2 as the coefficient dependent on distance. They used the term '$b_2$logr' as the sole distance dependent term and suggested that this term represents geometrical spreading for a simple point source model (b_1r-logr). However, this led to values of b_1 greater than zero. This result shows that ground motion attenuates less rapidly than 1/r, at least for distances less than 100 km. This is perhaps a result of the effect of critical-angle reflections from layers within and at the base of the crust (Boore *et al.* 1997). In this study, we applied a two-stage regression analysis utilizing the same equation form to western Anatolian strong motion data. Since there is no detailed information about near-surface velocities of the sites, the site classifications based on HVSR estimates as mentioned above were used.

Results

Our total data set consists of 168 recordings of ground motion from 49 earthquakes. Moment magnitudes of the earthquakes range between 4.0 and 6.4 while the hypocentral distance range is between 15 and 200 km (Figure 6). After applying the procedure described above, the following attenuation relationship was obtained for the largest PGA values between the two horizontal components:

$$\log y = 1.330095 + 0.640047\,(M-6) - 1.65663\log r + 0.14963S + 0.27P \quad (7)$$

S= 1 for site A and S= 0 for site B. The standard deviation, σ, is 0.27 and P is an 84% confidence level for the values of ±1σ. Distance and site condition dependent coefficients determined together with a set of amplitude factors for this model are listed in Table 4. In order to determine magnitude dependence, amplitude factors were regressed against magnitude values. All coefficients for the models of PGA and SA values and their standard errors along with the total and individual standard deviations of the regressions are given in Table 5. Since the standard errors are large for the actual values, significance levels of site coefficient for all periods were checked. As shown in Table 5, for the periods between 0.075 and 0.15 sec, the site coefficients are statistically significant at an 88–89% confidence level. As suggested by Equation 7 there is no quadratic term for dependence on magnitude, because the solution quality was not improved with the inclusion of this term at many of the period values.

The distribution of normalized residuals of the PGA values versus the distance, magnitude and predicted log(PGA) values are shown in Figure 7. In this figure, systematic trends were observed in the distribution of residuals, especially for site B residuals versus magnitude values. A similar trend was observed in the ratios between observed and predicted PGA values versus magnitude values for site B, although this trend lies within the ±1 standard deviation limits of the model (Figure 8). By examining this linear trend, the correction terms for the site coefficients were obtained. Table 6 lists Site Coefficient Correction (SCC) terms for different periods. F-test statistics reveal that there is no statistically meaningful trend between observed/predicted SA and magnitude values, at periods higher than 0.27 sec. After applying SCC term, the improvements on the distributions of the normalized residuals and the ratios between observed and predicted PGA values are shown in Figures 9 and 10, respectively. The ratios of observed/predicted SA values at period values of 0.15 and 0.5 sec for two different site classes without SCC term effect on site B are given in Figure 11. Figure 12 shows observed/predicted SA value ratios at a period of 0.25 sec for two different site classes and SCC term effect on site B.

Figure 13 compares predicted PGA values for M= 4.5, 5.0, 5.5 and 6.0 with observed PGA values. Predicted PGA values for M= 5.0, together with observed PGA values from the events 24 and 26

Table 4. The distance and site condition dependent coefficients determined along with a set of amplitude factors, by the first regression stage.

Coeff.	n	Values *(s.e.)*	Coefficient	n	Values *(s.e.)*	Coefficient	n	Values *(s.e.)*
A_1	1	1.072846 *(0.015)*	A_{18}	16	1.419449 *(0.058)*	A_{35}	7	0.93176 *(0.039)*
A_2	1	1.508271 *(0.015)*	A_{19}	3	0.017049 *(0.026)*	A_{36}	1	-0.03131 *(0.015)*
A_3	1	1.091626 *(0.015)*	A_{20}	16	0.824732 *(0.058)*	A_{37}	2	0.662295 *(0.021)*
A_4	1	1.271055 *(0.015)*	A_{21}	3	0.568507 *(0.026)*	A_{38}	2	0.613772 *(0.021)*
A_5	1	0.628728 *(0.015)*	A_{22}	1	-0.12039 *(0.015)*	A_{39}	2	-0.22189 *(0.021)*
A_6	2	1.412791 *(0.021)*	A_{23}	11	1.040472 *(0.049)*	A_{40}	1	0.485478 *(0.015)*
A_7	1	1.057449 *(0.015)*	A_{24}	13	0.58983 *(0.053)*	A_{41}	2	1.032605 *(0.021)*
A_8	2	0.355426 *(0.021)*	A_{25}	14	1.013113 *(0.054)*	A_{42}	1	0.211275 *(0.015)*
A_9	2	0.748027 *(0.021)*	A_{26}	8	0.544203 *(0.042)*	A_{43}	5	1.138124 *(0.033)*
A_{10}	2	0.709857 *(0.021)*	A_{27}	5	0.060287 *(0.033)*	A_{44}	2	1.074723 *(0.021)*
A_{11}	2	1.184064 *(0.021)*	A_{28}	2	0.306484 *(0.021)*	A_{45}	6	1.315589 *(0.037)*
A_{12}	2	0.900229 *(0.021)*	A_{29}	1	-0.0577 *(0.015)*	A_{46}	3	0.910989 *(0.026)*
A_{13}	2	0.550717 *(0.021)*	A_{30}	1	0.263145 *(0.015)*	A_{47}	1	0.144072 *(0.015)*
A_{14}	2	0.586012 *(0.021)*	A_{31}	3	0.800738 *(0.026)*	A_{48}	1	0.275192 *(0.015)*
A_{15}	2	0.935938 *(0.021)*	A_{32}	3	0.84045 *(0.026)*	A_{49}	4	0.701299 *(0.03)*
A_{16}	1	0.630462 *(0.015)*	A_{33}	1	0.448981 *(0.015)*	b	168	-1.65663 *(0.055)*
A_{17}	1	0.251075 *(0.015)*	A_{34}	1	0.448892 *(0.015)*	c	91	0.14963 *(0.098)*

n is total data number for each parameter. (s.e.) denotes standard errors of the coefficients (b_i) and obtained by using the well-known equation in where c_{ii} is the diagonal elements of variance-covariance matrix and s is the standard deviation values of the regression stages.

Table 5. The attenuation relationships coefficients to estimate 5% damped SA values (g) in western Anatolia. The entries for zero periods are the coefficients for PGA.

T (sec)	b *(s.e.)*	c *(s.e.)*	S.L.(c)	σ_1	a1 *(s.e.)*	a2 *(s.e.)*	σ_2	$\sigma_{log(Y)}$
0.00	-1.65663 *(0.055)*	0.14963 *(0.098)*	0.070	0.196	1.330095 *(0.068)*	0.640047 *(0.066)*	0.191	0.274
0.05	-1.58723 *(0.055)*	0.13127 *(0.098)*	0.100	0.197	1.28921 *(0.078)*	0.550356 *(0.073)*	0.214	0.291
0.0625	-1.55693 *(0.055)*	0.12721 *(0.098)*	0.102	0.198	1.272817 *(0.076)*	0.522723 *(0.072)*	0.210	0.289
0.075	-1.55269 *(0.055)*	0.12362 *(0.098)*	0.110	0.197	1.292287 *(0.078)*	0.501388 *(0.074)*	0.215	0.292
0.0875	-1.56996 *(0.055)*	0.12091 *(0.098)*	0.113	0.198	1.347802 *(0.075)*	0.490213 *(0.07)*	0.219	0.295
0.1	-1.59517 *(0.055)*	0.11772 *(0.098)*	0.120	0.199	1.427976 *(0.075)*	0.490708 *(0.07)*	0.209	0.289
0.125	-1.62299 *(0.056)*	0.11684 *(0.099)*	0.124	0.199	1.540824 *(0.073)*	0.51221 *(0.068)*	0.204	0.285
0.15	-1.64158 *(0.056)*	0.12453 *(0.1)*	0.110	0.201	1.604348 *(0.07)*	0.52885 *(0.067)*	0.200	0.283
0.175	-1.64675 *(0.056)*	0.1343 *(0.1)*	0.094	0.202	1.634407 *(0.074)*	0.54603 *(0.069)*	0.210	0.291
0.2	-1.64483 *(0.057)*	0.14763 *(0.101)*	0.077	0.204	1.643935 *(0.083)*	0.563768 *(0.08)*	0.220	0.300
0.225	-1.63362 *(0.058)*	0.16015 *(0.102)*	0.063	0.206	1.628 *(0.075)*	0.578914 *(0.072)*	0.211	0.295
0.25	-1.62417 *(0.058)*	0.16933 *(0.103)*	0.054	0.208	1.615247 *(0.073)*	0.594467 *(0.07)*	0.205	0.292
0.275	-1.61026 *(0.059)*	0.17721 *(0.104)*	0.050	0.209	1.590516 *(0.078)*	0.617139 *(0.073)*	0.223	0.306
0.3	-1.59306 *(0.06)*	0.18409 *(0.104)*	0.045	0.211	1.558349 *(0.078)*	0.630761 *(0.073)*	0.222	0.306
0.325	-1.58097 *(0.06)*	0.19134 *(0.105)*	0.034	0.212	1.531421 *(0.085)*	0.647707 *(0.08)*	0.242	0.322
0.35	-1.55999 *(0.061)*	0.20035 *(0.106)*	0.040	0.214	1.48272 *(0.082)*	0.657887 *(0.077)*	0.234	0.317
0.375	-1.54423 *(0.061)*	0.20801 *(0.107)*	0.030	0.216	1.435359 *(0.083)*	0.668748 *(0.078)*	0.237	0.321

Table 5 (Continued)

T (sec)	b *(s.e.)*	c *(s.e.)*	S.L.(c)	σ_1	a1 *(s.e.)*	a2 *(s.e.)*	σ_2	$\sigma_{\log(Y)}$
0.4	-1.52746 *(0.062)*	0.21302 *(0.108)*	0.028	0.218	1.389511 *(0.09)*	0.679789 *(0.085)*	0.245	0.328
0.425	-1.50273 *(0.062)*	0.21844 *(0.109)*	0.027	0.220	1.324814 *(0.097)*	0.690473 *(0.091)*	0.258	0.339
0.45	-1.47176 *(0.063)*	0.22561 *(0.11)*	0.024	0.222	1.251649 *(0.098)*	0.698052 *(0.092)*	0.261	0.343
0.475	-1.45552 *(0.063)*	0.22968 *(0.111)*	0.023	0.225	1.201875 *(0.095)*	0.705714 *(0.089)*	0.257	0.341
0.5	-1.42872 *(0.064)*	0.23198 *(0.112)*	*0.023*	0.226	1.134868 *(0.09)*	0.712904 *(0.084)*	0.249	0.336
0.6	-1.37063 *(0.065)*	0.23422 *(0.114)*	*0.024*	0.230	0.96091 *(0.093)*	0.740092 *(0.087)*	0.256	0.344
0.7	-1.3494 *(0.066)*	0.23557 *(0.116)*	*0.025*	0.233	0.839636 *(0.101)*	0.772522 *(0.095)*	0.274	0.360
0.8	-1.3409 *(0.067)*	0.2374 *(0.117)*	*0.025*	0.237	0.741725 *(0.105)*	0.793276 *(0.099)*	0.286	0.371
0.9	-1.34298 *(0.068)*	0.23828 *(0.119)*	*0.026*	0.240	0.667981 *(0.107)*	0.823529 *(0.1)*	0.290	0.376
1	-1.3461 *(0.069)*	0.23963 *(0.12)*	*0.027*	0.243	0.604281 *(0.108)*	0.845654 *(0.104)*	0.290	0.379
1.25	-1.33718 *(0.071)*	0.24146 *(0.124)*	*0.03*	0.251	0.495798 *(0.107)*	0.887541 *(0.103)*	0.296	0.388
1.5	-1.32902 *(0.074)*	0.24417 *(0.128)*	*0.032*	0.258	0.4198 *(0.112)*	0.921389 *(0.108)*	0.302	0.397
1.75	-1.33021 *(0.077)*	0.24505 *(0.131)*	*0.035*	0.265	0.366582 *(0.113)*	0.951321 *(0.108)*	0.299	0.400
2	-1.33122 *(0.079)*	0.24641 *(0.135)*	*0.038*	0.272	0.325294 *(0.108)*	0.987602 *(0.107)*	0.294	0.400

S.L.(c) represents significance level of site coefficient. $\sigma_{log(Y)}$ represents obtained final standard deviation. σ_1 and σ_2 are the standard deviations of the first and second regression stages, respectively. (s.e.) denotes standard errors of the coefficients.

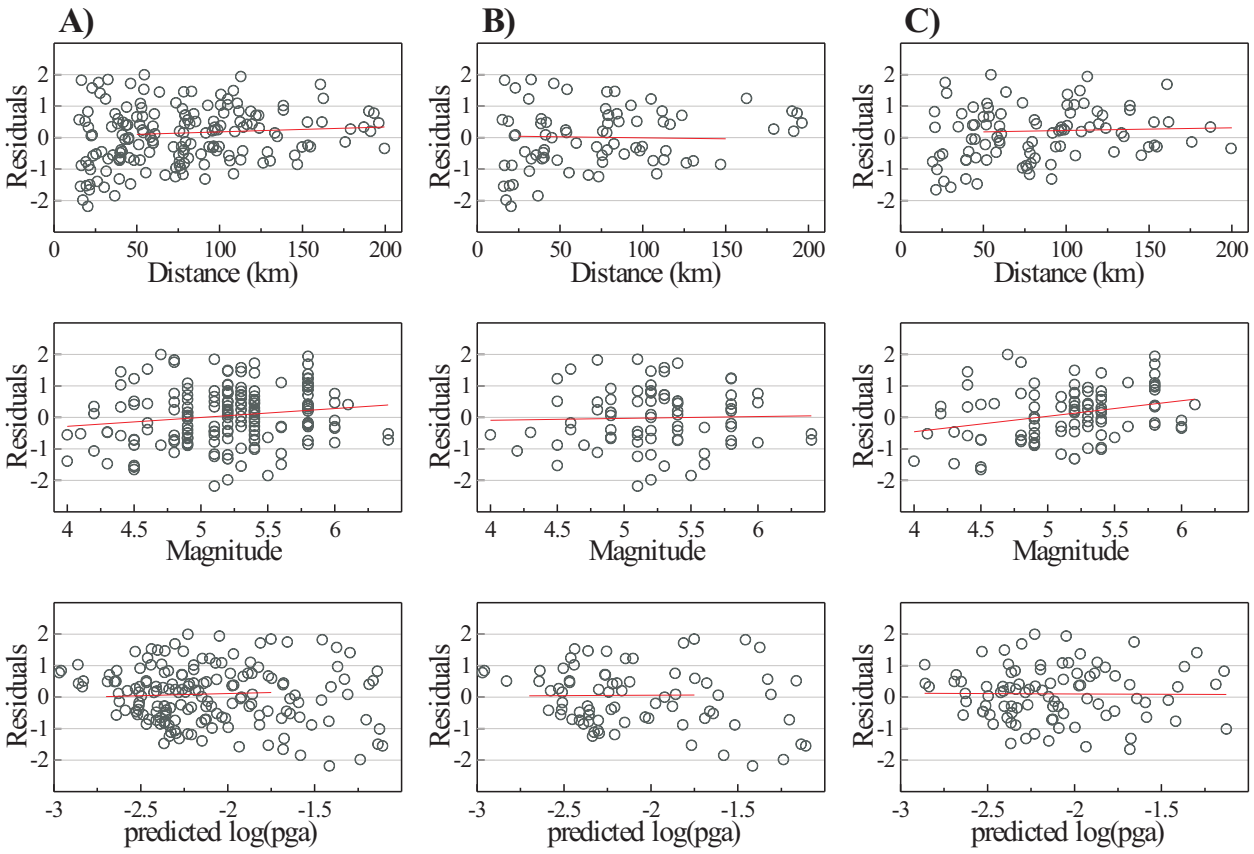

Figure 7. Distributions of the normalized residuals of the PGA values for **(a)** all data, **(b)** site A data and **(c)** site B data, versus the distance, magnitude and predicted log(PGA) values. Red lines represent linear trends.

(Buldan-2003 earthquakes, M= 4.9 and 5.1), and SA values for M= 6.0 at the period value of T= 0.25 sec together with observed SA values from the event 18 (Urla-2003 earthquake, M= 5.8) are given in Figure 14a and b, respectively. Predicted SA values for M= 4.5, 5.0, 5.5, 6.0 events and r_{hypo}= 15 km, are given in Figure 15. This figure also shows much better the SCC term effects versus the different magnitude values. Increasing values of amplitudes and dominant periods with increasing magnitude are observed in this figure. The effects of distance on predicted SA values are given in Figure 16. In this figure, predicted SA values for distances of 15, 20, 25, 30, 50 km and M= 6.0 are given. Decreasing amplitude values with increasing distance at all periods are observed in this figure as well as increasing dominant period values with increasing distance.

Comparison with Other Ground Motion Relationships

As mentioned above, different definitions for the predictor variables in attenuation relationships make them to be difficult to compare. But we tried to compare the predicted SA values with the models of Ambraseys *et al.* (1996) and Boore *et al.* (1997) which are based on the data from tectonically similar regions (Figure 17). The relationship of Ambraseys *et al.* (1996) was generated using a large data set from European strong motion records (hereafter referred to as AMB96). The equations were recommended for use in surface-wave magnitudes (M_S) ranging between 4.0 and 7.5 and for source distances up to 200 km. Their data set contained 422 records of 157 events in Europe and adjacent regions and three different site classes were utilized in this relationship: rock, stiff soil and soft soil. The relationship in Boore

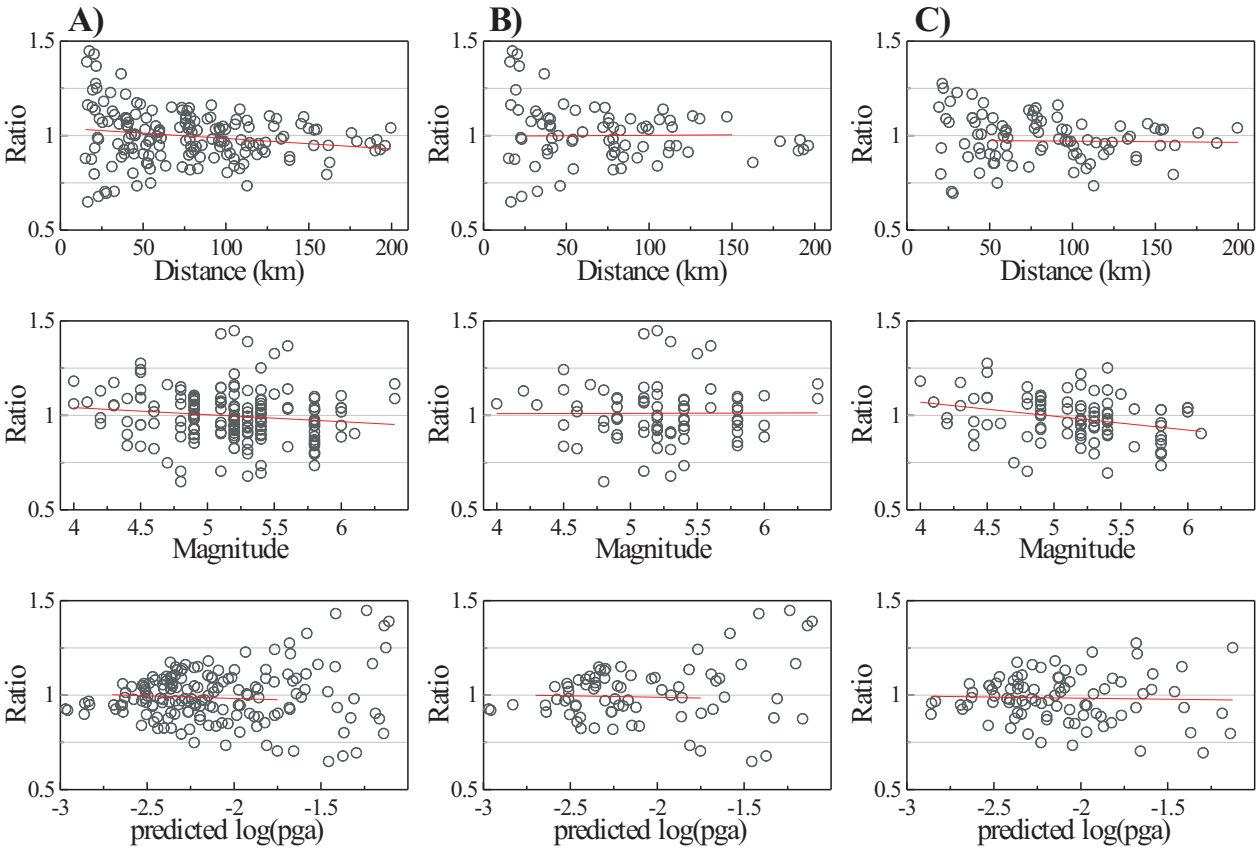

Figure 8. Distribution of the ratio between observed and predicted PGA values for **(a)** all data, **(b)** site A data and **(c)** site B data, versus the distance, magnitude and predicted log(PGA) values. Red lines represent linear trends.

et al. (1997) was obtained using strong motion records for shallow earthquakes in western North America (hereafter referred as BJF97). This relationship could be used to predict ground motions at distances within 80 km, and for M_w values between 5.5 and 7.5. The distance predictor was defined as r_{jb} in both models. Both of the relationships have a constant h parameter ('fictitious' depth measure, Boore *et al.* 1997) for each period value.

In order to compare the predicted SA values with the models of AMB96 and BJF97, an event with M_w= 6.0 and r_{jb}= 20 km was modelled (Figure 17). Since our distance predictor variable is hypocentral distance, in our model r_{hypo} was utilized as 22.4 km, by assuming that r_{hypo}= 22.4 km corresponds to an epicentral distance of 20 km, with focal depth of 10 km. Note that epicentral distance was used as r_{jb}, in order to compare the models. As described by the authors, M_S was used as a magnitude predictor variable in the AMB96 model. The site A and the site B models were compared with AMB96's stiff soil and soft soil models, respectively. In the BJF97 model, site condition predictors depend on the average velocities in the upper 30 metres of the crust. As shown in Figure 5, dominant frequencies at sites A and B are 4.71 and 2.0 Hz, respectively. According to the quarter-wavelength rule (Boore & Brown 1998), average velocities for the upper 30 m are 565 m/s and 240 m/s for the frequency values of 4.71 and 2 Hz, respectively. Utilizing these near-surface velocities and the BJM97 model, we predicted ground motion for sites A and B (Figure 17).

Comparison with the Turkish Building Code

In this study, we compared our models to SA models in the Turkish Building Code (hereafter referred as

Table 6. Site Coefficient Correction (SCC) terms for attenuation relationship models to account for soil nonlinearity effect.

T (sec)	Intercept *(s.e.)*	Slope *(s.e.)*	STS	S.L.
0	1.364 *(0.13)*	-0.0736 *(0.025)*	0.116	0.0045
0.05	1.5375 *(0.155)*	-0.1124 *(0.029)*	0.131	0.0002
0.0625	1.5815 *(0.161)*	-0.1215 *(0.031)*	0.137	0.0006
0.075	1.6174 *(0.183)*	-0.1288 *(0.035)*	0.151	0.0019
0.0875	1.6456 *(0.183)*	-0.1343 *(0.035)*	0.157	0.0005
0.1	1.6665 *(0.208)*	-0.1383 *(0.04)*	0.166	0.0015
0.125	1.688 *(0.202)*	-0.1417 *(0.039)*	0.169	0.0002
0.15	1.6851 *(0.228)*	-0.1397 *(0.044)*	0.188	0.0058
0.175	1.6608 *(0.216)*	-0.1333 *(0.042)*	0.19	0.0002
0.2	1.6183 *(0.212)*	-0.1231 *(0.041)*	0.179	0.0025
0.225	1.5608 *(0.193)*	-0.11 *(0.037)*	0.161	0.0014
0.25	1.4913 *(0.184)*	-0.0946 *(0.035)*	0.156	0.006
0.275	1.413 *(0.186)*	-0.0779 *(0.036)*	0.159	0.0589
0.3	1.3292 *(0.167)*	-0.0605 *(0.032)*	0.141	0.2563
0.325	1.2428 *(0.161)*	-0.0432 *(0.031)*	0.136	0.4751
0.35	1.157 *(0.169)*	-0.0269 *(0.033)*	0.147	0.3508
0.375	1.0751 *(0.169)*	-0.0122 *(0.033)*	0.148	0.4916

STS and S.L. represent standard deviations and significance level of fit, respectively. (s.e.) denotes standard errors of the coefficients.

TBC). In the TBC, the spectral acceleration model was defined as follows:

$$\begin{aligned} S(T) &= 1 + 1.5\ T / T_A && (0 \le T \le T_A) \\ S(T) &= 2.5 && (T_A < T \le T_B) \\ S(T) &= 2.5\ (T_B / T)^{0.8} && (T > T_B) \end{aligned} \qquad (8)$$

where, S(T) denotes normalized SA values for the PGA and T_A and T_B denote spectrum characteristic periods, depending on local site classes.

Definitions of local site classes and soil groups utilizing site classification in the TBC are given in Tables 7 and 8, respectively. As shown in equation 8, period values are the only independent variables here. Comparisons of obtained models with SA models in the TBC are given in Figures 18 and 19. Figure 18 shows a decrease of the largest SA/PGA values against increasing magnitude. The effects of distance on predicted normalized SA values are given in Figure 19, where the largest SA/PGA and dominant period values increase with distances.

Discussion

Our results show that predicted PGA and 5%-damped SA values correlate well with the observed values. Only for the closer events (r_{hypo}< 25 km) were larger residuals observed between measured and predicted values, possibly because of rupture directivity effects. However, no parameter accounting for rupture directivity was included in the model used in this study.

As shown in Figure 5, dominant frequencies of the site A and B classes are 4.71 and 2.0 Hz. According to the quarter-wavelength rule (Boore & Brown 1998), average velocities for the upper 30 m are 565 m/s and 240 m/s for frequencies of 4.71 and 2 Hz, respectively. These velocities correspond to sites C and D in the NEHRP site categories. For those reasons, sites A and B should be evaluated as stiff soil and soil sites in the region. 54% and 46% respectively of data in the dataset actually comes from sites A and B classes. Data from sites 1 and 2 were combined and designated as data from site A. Similarly, data from sites 3 and 4 were combined and designated as data

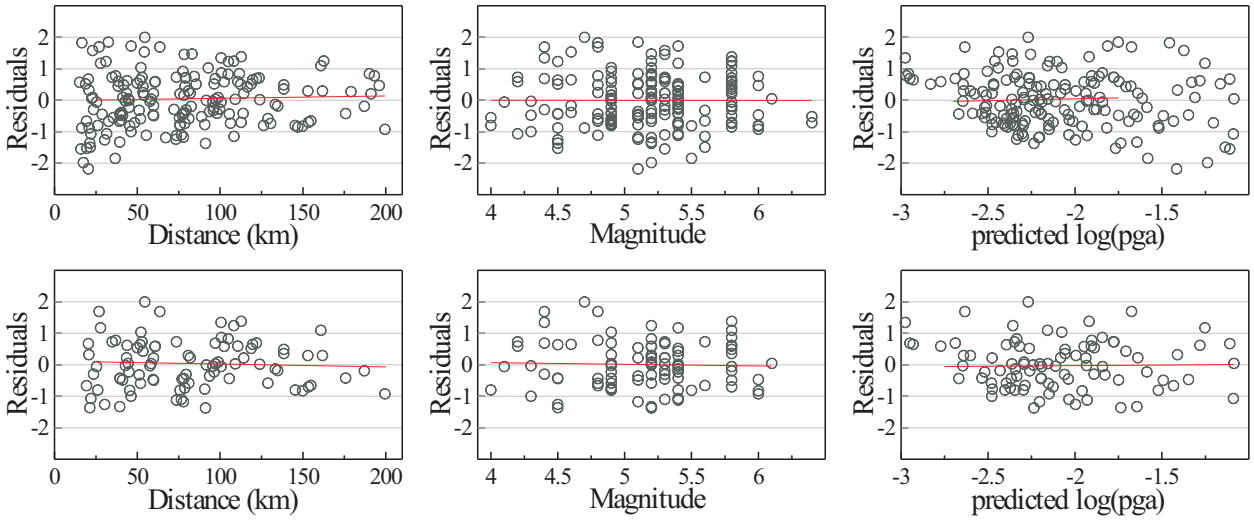

Figure 9. Distributions of normalized residuals of the PGA model, including the SCC term effect, top graphs for all data and bottom graphs for site B data, versus the distance, magnitude and predicted log(PGA) values. Red lines represent linear trends.

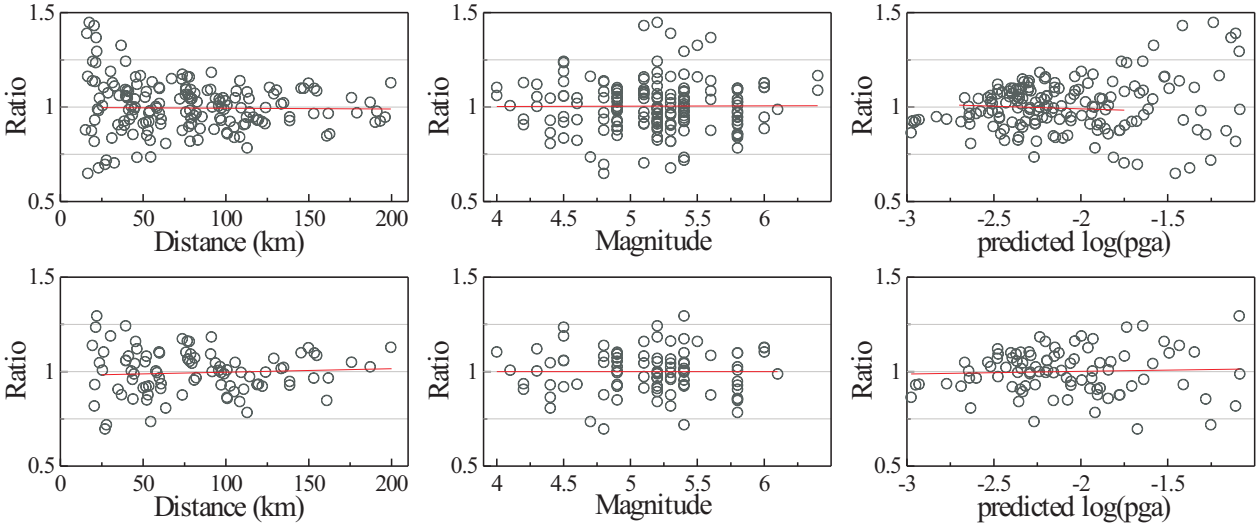

Figure 10. Distribution of the ratios between observed and predicted PGA, including the SCC term effect, top graphs for all data and bottom graphs for site B data, versus the distance, magnitude and predicted log(PGA) values. Red lines represent linear trends.

from site B (Figure 5) in the regression analysis. As shown in Table 2, 65% of the data is from site 4 (deep soil) in site B (deep soil) and 74% of the data is from site 2 (stiff soil) in site A.

Predicted 5%-damped SA values have shown that soil/deep soil amplifications are significant in the region. For site A, dominant periods of M= 4.5, 5.0, 5.5 and 6.0 events are about 0.15, 0.17, 0.19 and 0.2 while these values are about 0.18, 0.21, 0.25, 0.31 and 0.32 for site B, respectively (Figure 15). These results show that deep basin effects and weakness of basin fill materials are significant in the graben systems of

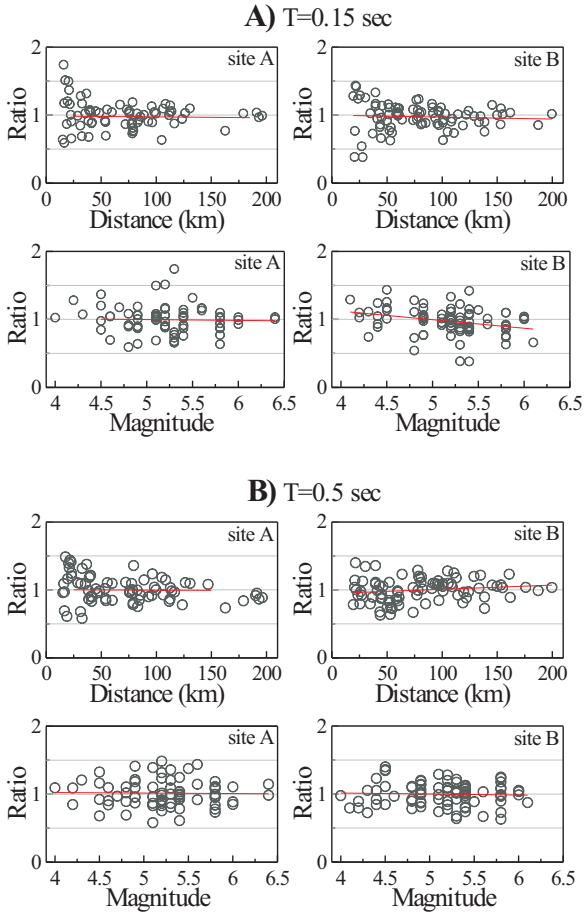

Figure 11. The ratio between observed and predicted SA values at the period values of **(a)** 0.15 and **(b)** 0.5 sec for site A and B classes without the SCC term effect. Red lines represent linear trends.

western Anatolia. Geological observations suggest that the Neogene sediments in the Gediz Graben (GG, in Figure 2) are about 1.3–1.5 km thick, measured at the detachment fault, which forms the contact between the Neogene sediments and metamorphic rocks (Bozkurt & Sözbilir 2004). Analysis of gravity data revealed that the maximum thickness of sedimentary cover is between 2.5 and 3.5 km in the Büyük Menderes Graben (BMG, in Figure 2), and between 0.5 and 2.0 km in the Gediz Graben (GG, in Figure 2) (Sarı & Şalk 2006). Another reason for the large dominant periods could be saturated soil deposits in the region: the low crustal velocities in the region are associated with a high degree of fracturing and the presence of fluids at high pressure in the crust by Akyol *et al.* (2006). Shean-Der *et al.* (1997) showed that the saturated soil deposit has a smaller surface amplitude and significantly lower resonant frequency than an unsaturated soil deposit of the same thickness.

Figure 16 shows lengthening of the dominant periods and rapid decrease in the amplitudes with increasing distance. This rapid decrease is consistent with the reported high seismic attenuation for western Anatolia. Studies of attenuation of regionally recorded coda waves (Akıncı *et al.* 1994) and Lg waves (Akıncı *et al.* 1995) have indicated that crustal seismic wave attenuation is high in the region. Tomographic studies of Lg coda Q have implied that attenuation values in western Anatolia are among the highest in all Eurasia (Mindevalli & Mitchell 1989; Cong & Mitchell 1999; Mitchell *et al.* 2008).

As shown in Figures 15 and 16, magnitude-dependent SCC terms cause lower estimates for larger events and higher estimates for smaller events at lower periods. The existence of this term implies nonlinearity of deep soil sites in the region. According to Field (2000), if nonlinear effects are significant at higher levels of shaking, they will probably manifest themselves as an under-prediction of rock-site PGA rather than an over-prediction of sediment-site PGA. Due to data limitations, we could not examine whether or not soil nonlinearity effects occur for site A. However, results obtained for site B show that soil nonlinearity effects at lower periods (≤ 0.27 sec) are significant at higher levels of shaking and manifest over-prediction of sediment-site acceleration values while they manifest lower prediction at lower levels of shaking. Amplification occurs due to low-velocity deposits and resonances in the soil column. At higher levels of shaking at site B, nonlinearity attenuates periods less than 0.27 second due to the increased damping in the soil column. However, at longer periods, amplification within the soil column controls site behavior and produces larger SA values.

Figure 17 shows comparisons of the predicted SA values with the models of AMB96 and BJF97. Three models based on our site A class are consistent, except for SA values at larger periods of the AMB96 model. For both site classes long-period values (T>1.5 sec), AMB96 model predictions are lower than the others. Figure 17 shows discrepancies

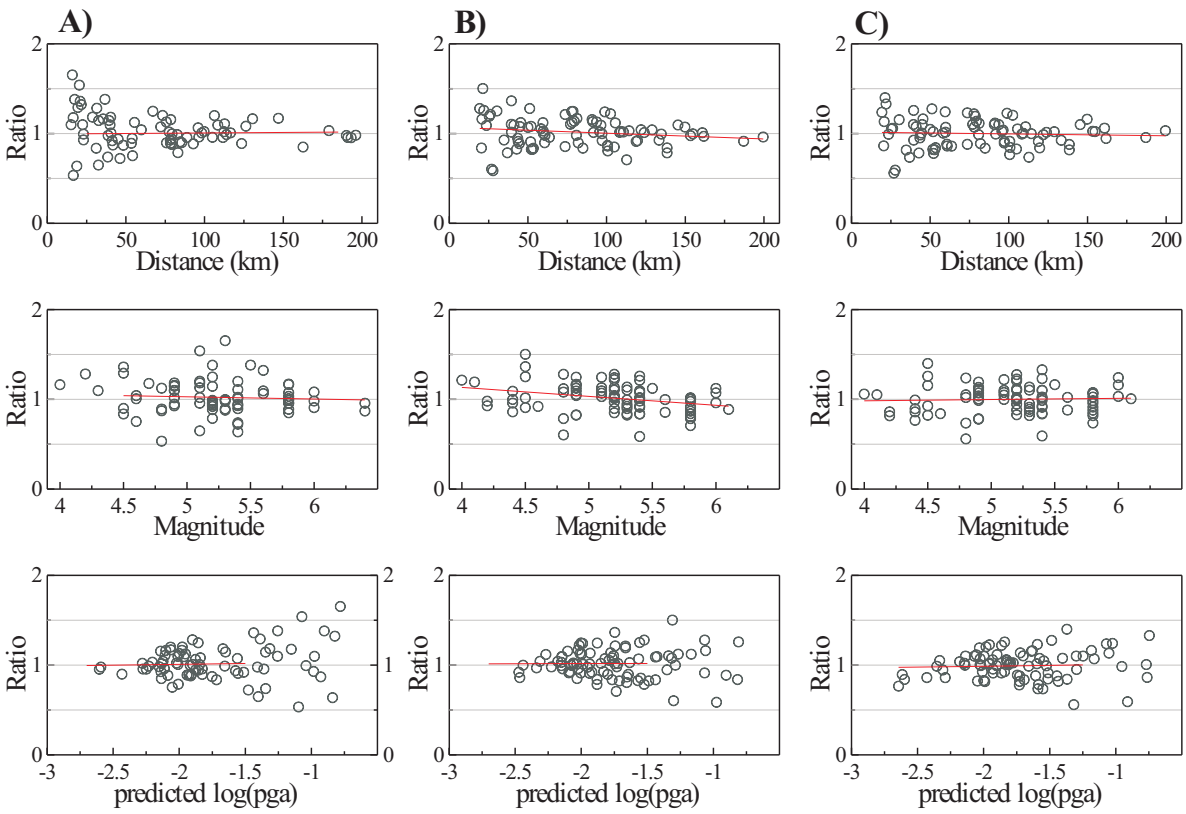

Figure 12. The ratio between observed and predicted SA values at a period value of 0.25 sec for **(a)** site A, **(b)** site B without the SCC term effect and **(c)** site B with the SCC term effect. Red lines represent linear trends.

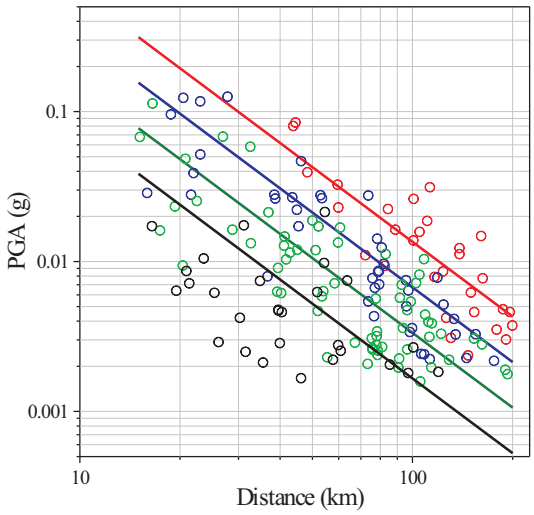

Figure 13. Predicted PGA values for M= 4.5, 6.0, 5.5 and 6.0 events, represented by black, green, blue and red lines, respectively. Black, green, blue and red circles represent observed data from 4.00≤M<4.75, 4.75≤M<5.25, 5.25≤M<5.75 and 5.75≤M events, respectively.

between three models based on our site B class. Our predicted values are smaller at short period values while they are larger at medium periods. While the SCC term was not accounted in our model, the three models are consistent at short periods. Nevertheless, none of the AMB96 and BJF97 models account for that effect. Field (2000) reported that the BJF97 model does not explicitly account for the nonlinear sediment effect. Larger predictions for medium periods suggest that site amplifications in the region and the basin effect are stronger than in other regions. However, because the physical mechanism for the basin effect has still been discussed and because different procedures were used by different workers any interpretation regarding with this comparison would be premature. For example, the BJF97 model was obtained using data that was averaged between two horizontal components. That can cause smaller SA values generated by the model. Anderson (2000) suggested that the distance

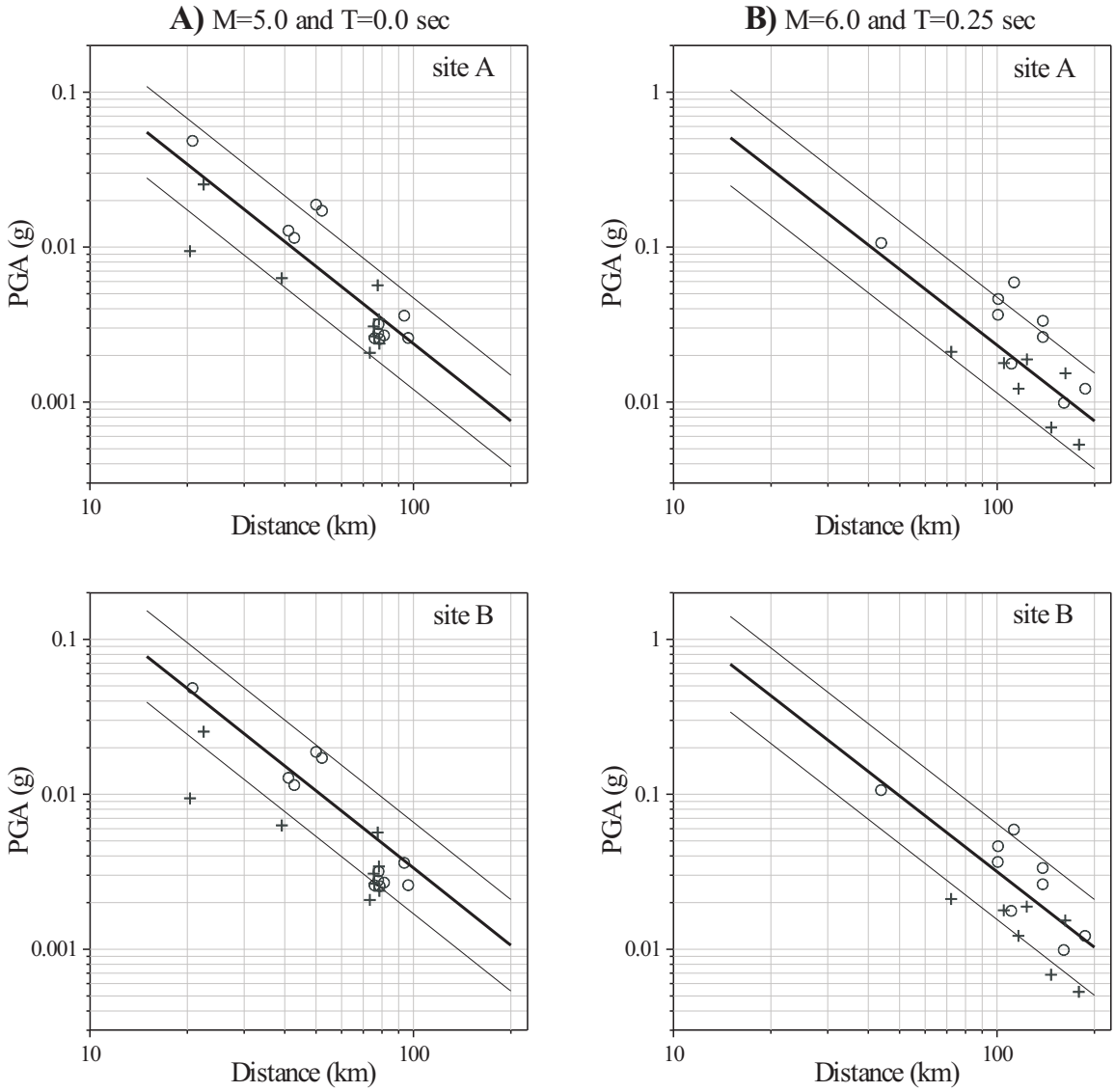

Figure 14. **(a)** Predicted PGA values for M= 5.0 event together with observed PGA values from the events 24 and 26 (Buldan-2003 earthquakes, M= 4.9 and 5.1, respectively) and **(b)** SA values for M= 6.0 event at the period value of T= 0.25 sec together with observed SA values from the event 18 (Urla-2003 earthquake, M= 5.8). Predicted values and their ±1 standard deviations are represented by thick and thin black lines, respectively. Crosses and circles represent observed data from site A and B classes, respectively.

dependency does not vary with magnitude in the BJF97 model. On the other hand, the dataset of Ambraseys *et al.* (1996) was taken from very large region including Europe and its environs in order to utilize attenuation relationships. Lee (1997) discussed the uncertainties in the AMB96 model. In brief, all the relationships generated by the workers have been obtained by different definitions and procedures in various equation forms.

Comparison of the obtained results with the SA models in TBC has been shown that it is not possible to categorize the site A and B classes according to the

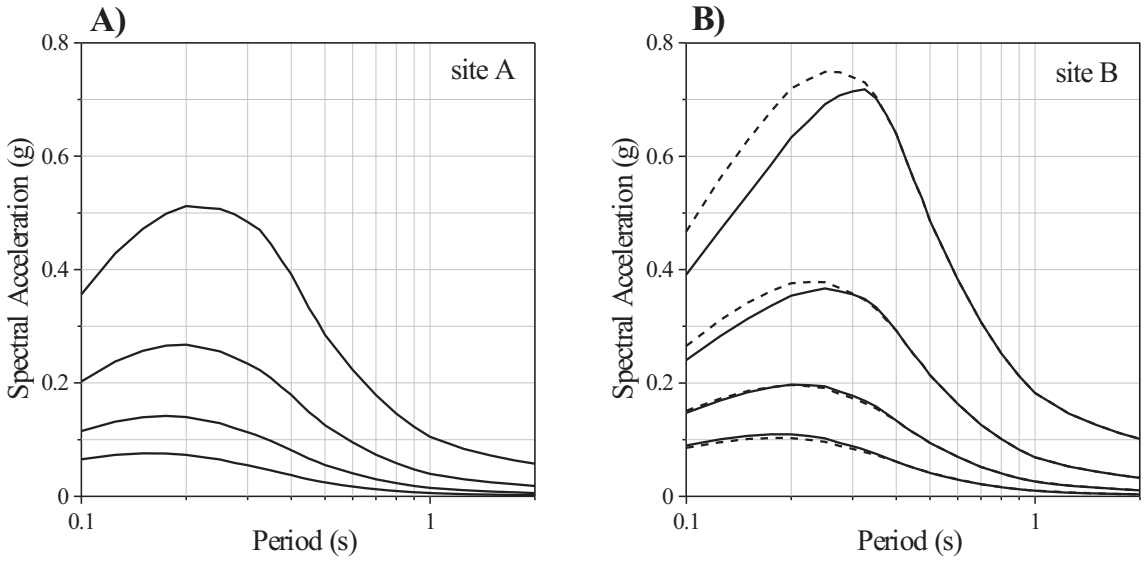

Figure 15. The effects of magnitude on SA values of **(a)** site A and **(b)** site B classes for r_{hypo}= 15 km and M= 6.0, 5.5, 5.0, 4.5 events. Amplitudes decrease with decreasing magnitude values. Dashed lines represent predictions without the SCC term effect.

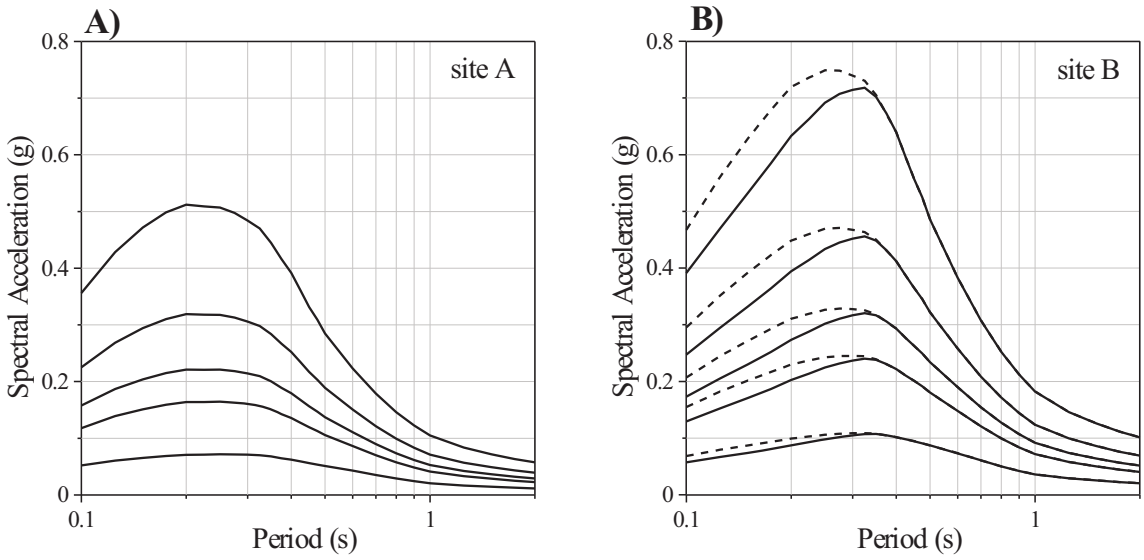

Figure 16. The effects of distance on SA values of **(a)** site A and **(b)** site B classes for M= 6.0 event and r_{hypo}= 15, 20, 25, 30, 50 km. Amplitudes decrease with increasing distance values. Dashed lines represent predictions without the SCC term effects.

TBC local site classification (Table 7) (Figures 18 &19). The site A and B classes correspond to soil groups B and C in TBC (Table 8). The SA/PGA amplitude values for smaller events (M<5) are higher than the top level of the SA models in the TBC (Figure 18). A reason of this higher prediction could be lower prediction of PGA values. Nevertheless, our results imply that the observed and modeled PGA

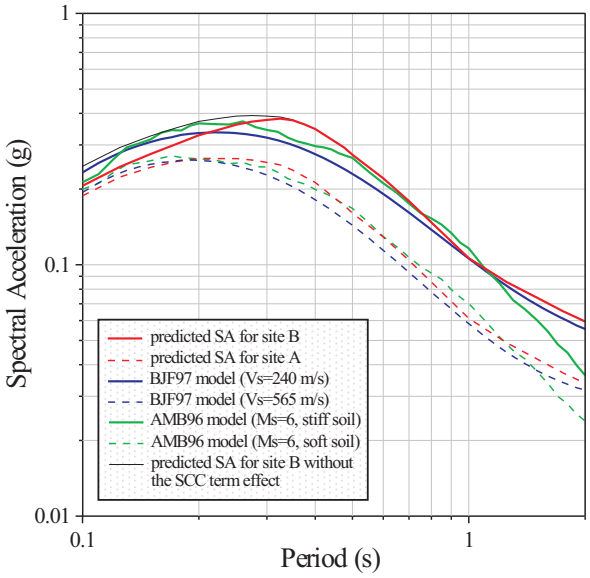

Figure 17. Comparison of the predicted SA values with the models of AMB96 and BJF97 for an event with M_w=6.0 and r_{jb} =20 km. Red, blue and green solid lines represent predictions for site B from the models of this study, BJF97 and AMB96, respectively. Dashed lines represent predictions for the site A. The prediction without the SCC term effect is shown as a thin black line.

values are consistent (Figures 9, 10 & 13). On the other hand, because of small SA values generated by those smaller events (Figure 15), they are less important from an engineering point of view. As shown in Figure 19, increasing amplitudes with increasing distance (greater than 50 km) in the models will cause higher predicted SA/PGA values than the TBC model, especially for the site B class. This result implies that the SA model in TBC may not result from deep basin effects at larger distances.

In this study, we tried to eliminate most of the sources of uncertainty in the regression analysis. For example, HVSR estimates were used for site classification, hypocentral distance was used as the distance predictor variable to eliminate the errors in the location processes and the source zone definition, while the form of the attenuation relationship has been chosen with regard to the dataset limitations. The standard errors for determined coefficients were given in detail because uncertainties are brought into the regression analysis with the usage of magnitude values reported by different institutes/works and limited data.

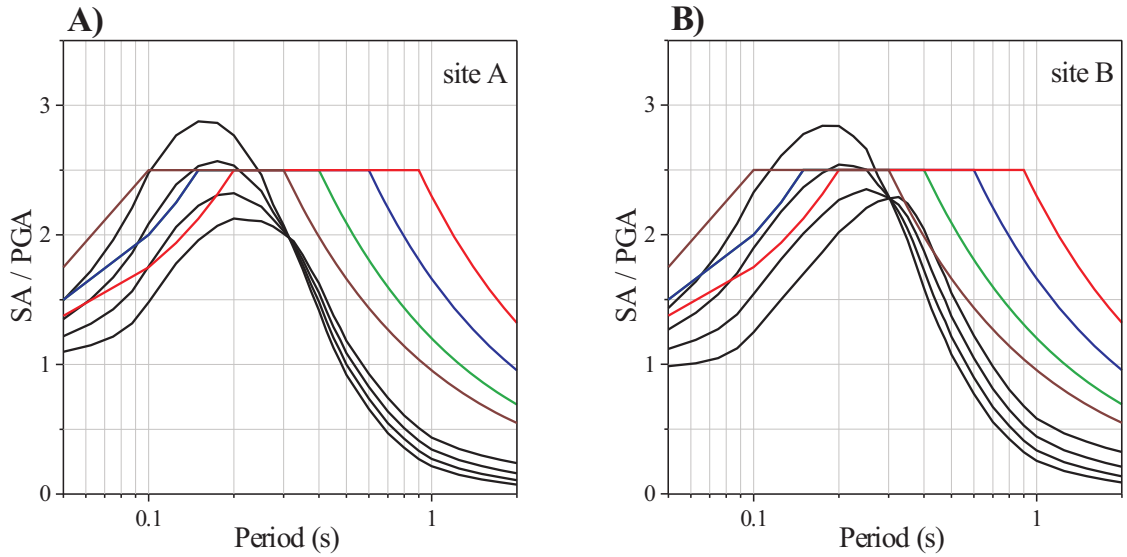

Figure 18. Comparison of obtained models with the SA models in the TBC. Predicted SA/PGA values for M= 4.5, 5.0, 5.5, 6.0 events and r_{hypo}= 15 km (black lines) for **(a)** site A and **(b)** site B. A decrease in the largest SA/PGA value with increasing magnitude was observed. Red, blue, green and brown lines represent Z4, Z3, Z2 and Z1 site classes in the TBC, respectively.

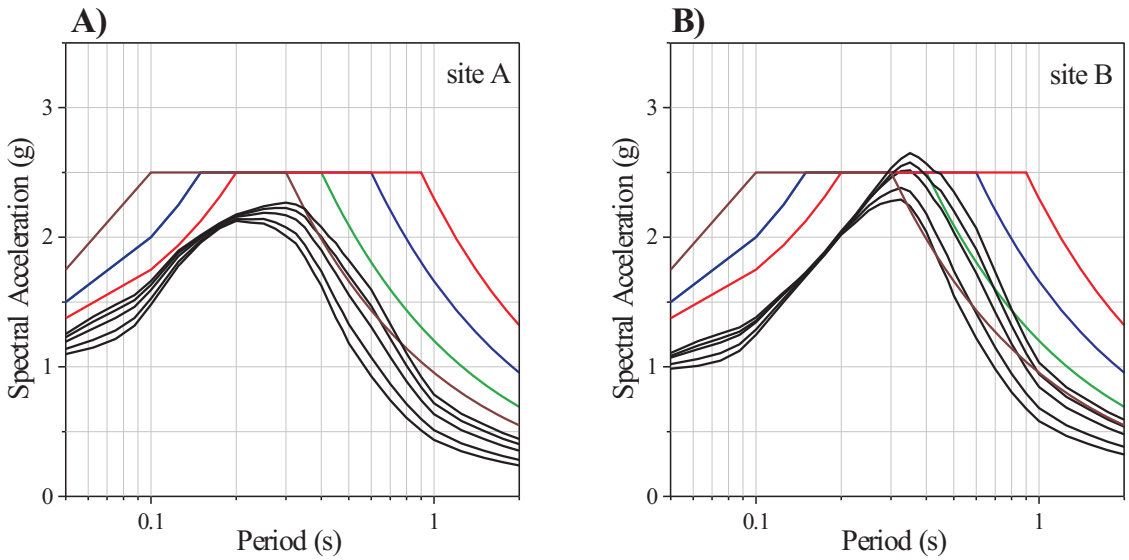

Figure 19. Comparison of obtained models with the SA models in the TBC. Predicted SA/PGA values for M= 6.0 event and r_{hypo}= 15, 25, 50, 75, 100 km (black lines) for **(a)** site A and **(b)** site B. An increase in the largest SA/PGA and dominant period values with increasing distance was observed. Red, blue, green and brown lines represent Z4, Z3, Z2 and Z1 site classes in the TBC, respectively.

Table 7. Local Site Classes defined in the Turkish Building Code.

Local Site Class	Soil Group and Topmost Layer Thickness (h1)	TA(sec)	TB(sec)
Z1	Group A soils and Group B soils with h1≤15 m	0.10	0.30
Z2	Group B soils with h1>15 m and Group C soils with h1 ≤15 m	0.15	0.40
Z3	Group C soils with 15 m < h1≤50 m and Group D soils with h1≤10 m	0.15	0.60
Z4	Group C soils with h1>50 m and Group D soils with h1>10 m	0.2	0.9

Table 8. Soil Groups defined in the Turkish Building Code.

Soil Group	Description of Soil Group	V_S (m/s)
A	1. Massive volcanic rocks, unweathered sound metamorphic rocks, stiff cemented sedimentary rocks 2. Very dense sand, gravel,... 3. Hard clay, silty clay,…	> 1000 > 700 > 700
B	1. Soft volcanic rocks such as tuff and agglomerate, weathered cemented sedimentary rocks with planes of discontinuity,… 2. Dense sand, gravel,… 3. Very stiff clay, silty clay,…	700–1000 400–700 300–700
C	1. Highly weathered soft metamorphic rocks and cemented sedimentary rocks with planes of discontinuity 2. Medium dense sand and gravel,… 3. Stiff clay, silty clay,…	400–700 200–400 200–300
D	1. Soft, deep alluvial layers with high water table,… 2. Loose sand,… 3. Soft clay, silty clay,…	< 200 < 200 < 200

Conclusions

The largest peaks between the two horizontal components and 5%-damped spectral acceleration values of 168 recordings for 49 earthquakes were used to obtain empirical attenuation relationships for western Anatolia. The moment magnitude range of earthquakes in the data set, is between 4.0 and 6.4 while the hypocentral distance range is between 15 and 200 km. Obtained model coefficients should be used for these ranges of magnitude and distance.

The results of HVSR estimates used in the site classification and the regression analysis used to obtain attenuation relationships have shown that deep soil amplifications are significant in the region. Not only large earthquakes but also moderate sized ones in the region are the dominant source of seismic hazard, because of their larger amplitude at longer periods in deep basin structures of the western Anatolia graben system.

Our inferred attenuation relation model explicitly accounts for nonlinear behaviour of soil sites in the region. The nonlinear effects of soil/deep soil sites at lower periods (≤ 0.27 sec) are significant at higher levels of shaking and manifest over prediction of sediment-site acceleration values while they manifest lower prediction at lower levels of shaking.

Our results show that most of the strong motion stations in the region are located on soil sites. To better compare rock and soil sites, the number of the stations located on the rock sites in the region should be increased. The results also show that the present soil classification for strong motion sites in Turkey should be re-evaluated in detail.

Comparisons of the results with the attenuation relationships based on data from tectonically similar regions have shown that ground motion attenuation relationships modelled for a specific region cannot normally be used in engineering analysis for other regions. The ground motion levels can differ even in similar tectonic regimes, since these levels are related not only to tectonics but also to the actual physical attributes of the region. The results also indicate that the TBC models cannot explain magnitude and distance dependencies adequately if only the period values are used as independent variables.

In this study, we determined initial attenuation relationships for western Anatolia. Previously strong motion data have not been sufficiently abundant to utilize the regression procedures to constrain the distance and magnitude dependence of ground motion in the frequency range that is responsible for earthquake damage. The data from two different networks (TNSMN and WASRE) were merged for this purpose. It is hoped that this study will guide future developments and provide an interim solution until updated models become available. However, standard deviations of the obtained relationships should be taken into account if the results are going to be utilized for engineering applications. More precise modeling will be possible when much more data and information become available for the region. For that reason, well-distributed strong motion networks, as well as detailed studies of the site conditions and the source geometries, are needed for seismic hazard studies in western Anatolia.

Acknowledgments

The authors are grateful to Tuncay Taymaz and an anonymous reviewer for their dedicated support and constructive criticisms, which significantly improved the manuscript. The authors would like to thank Ertuğrul Benzeden, Brian J. Mitchell, Mustafa Ergün, Mine Orgun, Murat Çamyıldız and Türker Yas for their contributions. English of the final text is edited by John A. Winchester.

References

Abrahamson, A.A. & Shedlock, K.M. 1997. Overview. *Seismological Research Letters*, **68**, 9–23.

Abrahamson, N.A. & Silva, W.J. 1997. Empirical response spectral attenuation relations for shallow crustal earthquakes. *Seismological Research Letters* **68**, 94–127.

Akinci, A., Ibanez, J.M., Del Pezzo, E. & Morales, J. 1995. Geometrical spreading and attenuation of Lg waves: a comparison between Western Anatolia (Turkey) and Southern Spain. *Tectonophysics* **250**, 47–60.

Akinci, A., Taktak, A.G. & Ergintav, S. 1994. Attenuation of coda waves in Western Anatolia. *Physics Earth and Planet Interior* **87**, 155–165.

Akyol, N., Akinci, A. & Eyidoğan, H. 2002. Site amplification of S-waves in Bursa city and its vicinity, northwestern Turkey: comparison of different approaches. *Soil Dynamics and Earthquake Engineering* **22**, 579–587.

Akyol, N., Zhu, L., Mitchell, B.J., Sözbilir, H. & Kekovali K. 2006. Crustal structure and local seismicity in Western Anatolia. *Geophysical Journal International* **166**, 1259–1269, doi: 10.1111/j.1365-246X.2006.03053.x.

Ambraseys, N.N., Simpson, K.A. & Bommer, J.J. 1996. Prediction of horizontal response spectra in Europe. *Earthquake Engineering and Structural Dynamics* **25**, 371–400.

Anderson, J.G. 2000. Expected shape of regressions for ground-motion parameters on rock. *Bulletin Seismological Society of America* **90**, 43–52.

Atkinson, G.M. & Boore, D.M. 1997. Stochastic point-source modeling of ground motions in the Cascadia region. *Seismological Research Letters* **68**, 74–85.

Barka, A. & Reilinger, R. 1997. Active tectonics of the Eastern Mediterranean region: deduced from GPS, neotectonic and seismicity data. *Annali Geofisica* **40**, 587–610.

Bindi, D., Luzi, L., Pacor, F., Franceschina, G. & Castro, R.R. 2006. Ground-motion predictions from empirical attenuation relationships versus recorded data: the case of the 1997–1998 Umbria-Marche, central Italy, strong-motion data set. *Bulletin Seismological Society of America* **96**, 984–1002, doi: 10.1785/0120050102.

Boore, D.M. & Brown, L.T. 1998. Comparing shear-wave velocity profiles from inversion of surface-wave phase velocities with downhole measurements: systematic differences between the CXW method and downhole measurements at six USC strong-motion sites. *Seismological Research Letters* **69**, 222–229.

Boore, D.M., Joyner, W.B. & Fumal T.E. 1997. Equations for estimating horizontal response spectra and peak acceleration from Western North American earthquakes: a summary of Recent work. *Seismological Research Letters* **68**, 128–153.

Bozkurt, E. 2000. Timing of extension on the Büyük Menderes Graben, Western Turkey, and its tectonic implications. *In*: Bozkurt, E., Winchester, J.A. & Piper, J.D.A. (eds), *Tectonics and Magmatism in Turkey and the Surrounding Area*. The Geological Society, London, Special Publications **173**, 385–403.

Bozkurt, E. 2001. Neotectonics of Turkey – a synthesis. *Geodinamica Acta* **14**, 3–30.

Bozkurt, E. 2003. Origin of NE-trending basins in Western Turkey. *Geodinamica Acta* **16**, 61–81.

Bozkurt, E. & Sözbilir, H. 2004. Tectonic evolution of the Gediz Graben: field evidence for an episodic, two-stage extension in Western Turkey. *Geological Magazine* **141**, 63–79.

Campell, W.K. 1997. Empirical near-source attenuation relationships for horizontal and vertical components of peak ground acceleration, peak ground velocity and pseudo-absolute acceleration response spectra. *Seismological Research Letters* **68**, 154–179.

Cong, L. & Mitchell, B.J. 1999. Lg Coda Q and its relation to the geology and tectonics of the Middle East. *Pure and Applied Geophysics* **153**, 563–585.

Draper, N.R. & Smith, H. 1966. *Applied Regression Analysis*. Wiley, New York.

Field, E.H. 2000. A modified ground-motion attenuation relationship for southern California that accounts for detailed site classification and a basin-depth effect. *Bulletin Seismological Society of America* **90**, 209–221.

Gülkan, P & Kalkan, E. 2002. Attenuation modeling of Recent earthquakes in Turkey. *Journal of Seismology* **6**, 397–409.

Gregor, N., Silva, W.J., Wong, I.G. & Youngs, R.R. 2002. Ground-motion attenuation relationships for Cascadia subduction zone mega-thrust earthquakes based on a Stochastic Finite Source. *Bulletin Seismological Society of America* **92**, 1923–1932.

Joyner, W.B. & Boore, D.M. 1981. Peak horizontal acceleration and velocity from strong-motion records including records from the 1979 Imperial Valley, California, earthquake. *Bulletin Seismological Society of America* **71**, 2011–2038.

Joyner, W.B. & Boore, D.M. 1993. Methods for the regression analysis of strong-motion data. *Bulletin Seismological Society of America* **83**, 469–487.

Kiratzi, A.A. & Louvari, E.K. 2001. On the active tectonics of the Aegean Sea and the surrounding lands. *In*: Taymaz, T. (eds), *Proceedings of Symposia on Seismotectonics of the North-Western Anatolia-Aegean and Recent Turkish Earthquakes*, 88–95, İstanbul Technical University, Turkey.

Koçyiğit, A., Yusufoğlu, H. & Bozkurt, E. 1999. Evidence from the Gediz Graben for episodic two-stage extension in Western Turkey. *Journal of the Geological Society* **156**, 605–616.

Konak, N. & Şenel, M. 2002. *Geological Map of Turkey at 1:500000 Scale*. General Directorate of Mineral and Research Exploration of Turkey Publications.

Kramer, S.L. 1996. *Geotechnical Earthquake Engineering*. Prentice Hall. Inc., Upper Saddle River, New Jersey.

Lachet, C., Hatzfeld, D., Bard, P.Y., Theodulidis, N., Papaioannou, C. & Savvaidis, A. 1996. Site effects and microzonation in the city of Thessaloniki (Greece): comparison of different approaches. *Bulletin Seismological Society of America* **86**, 1692–1703.

Lee, V.W. 1997. Discussion on 'Prediction of horizontal response spectra in Europe'. *Earthquake Engineering and Structural Dynamics* **26**, 289–293.

Mindevalli, Y.Ö. & Mitchell, B.J. 1989. Crustal structure and possible Anisotropy in Turkey form seismic surface wave dispersion. *Geophysical Journal International* **98**, 93–106.

Mitchell, B.J., Cong, L. & G. Ekström, G. 2008. A continent-wide map of 1-Hz *Lg* Coda *Q* variation across Eurasia and its relation to lithospheric evolution. *Journal of Geophysical Research* **113**, B04303, doi:10.1029/2007JB005065.

Özbey, C., Sari, A., Manuel, L., Erdik, M. & Fahjan, Y. 2004. An empirical attenuation relationship for northwestern Turkey ground motion using a Random Effects Approach. *Soil Dynamics and Earthquake Engineering* **24**, 115–125.

Sadigh, K., Chang, C.Y., Egan, J.A., Makdisi, F. & Youngs, R.R. 1997. Attenuation relationships for shallow crustal earthquakes based on California Strong Motion Data. *Seismological Research Letters* **68**, 180–189.

Sari, C. & Şalk, M. 2006. Sediment thicknesses of the Western Anatolia graben structures determined by 2D and 3D analysis using gravity data. *Journal of Asian Earth Sciences* **26**, 39–48.

Saunders, P., Priestley, K. & Taymaz, T. 1998. Variations in the crustal structure beneath Western Turkey. *Geophysical Journal International* **134**, 373–389.

Shean-Der, N., Siddharthan, V. & Anderson, J.G. 1997. Characteristics of nonlinear response of deep saturated soil deposits. *Bulletin Seismological Society of America* **87**, 342–355.

Spudich, P., Flecther, J.B., Hellweg, M., Boatwright, C., Sullivan, C., Joyner, W.B., Hanks, T.C., Boore D.M., Mcgarr A., Baker L.M. & Lindh A.G. 1997. SEA96 – a new predictive relation for earthquake ground motions in extensional tectonic regimes. *Seismological Research Letters* **68**, 190–198.

Şaroğlu, F., Emre, Ö. & Kuşcu, İ. 1992. *Active Fault Map of Turkey*. General Directorate of Mineral and Research Exploration of Turkey Publication.

Şengör, A.M.C. 1987. Cross-faults and differential stretching of hanging walls in regions of low-angle normal faulting: examples from Western Turkey. *In*: Coward, M.P., Dewey, J.F. & Hancock, P.L. (eds), *Continental Extensional Tectonics*. The Geological Society, London Special Publications **28**, 575–589.

Şengör, A.M.C., Görür, N. & Şaroğlu F., 1985. Strike-slip faulting and related basin formations in zones of tectonic escape: Turkey as a case study. *In*: Biddle, K.T. & Christie-Blick, N., *Strike-slip Faulting and Basin Formation*. Society of Economic Paleontologits and Mineralogists, Special Publications **37**, 227–264.

Tan, O. & Taymaz, T. 2006. Active tectonics of the Caucasus: earthquake source mechanisms and rupture histories obtained from inversion of teleseismic body waveforms. *In*: Dilek, Y. & Pavlides, S. (eds), *Postcollisional Tectonics and Magmatism in the Mediterranean Region and Asia.* Geological Society of America Special Paper **409**, 531–578, doi: 10.1130/2006.2409(25).

Taymaz, T. 1993. The source parameters of Çubukdağ (Western Turkey) earthquake of 11 October 1986. *Geophysical Journal International* **113**, 260–267.

Taymaz, T., Jackson, J.A. & Westaway, R. 1990. Earthquake mechanisms in the Hellenic trench near Crete. *Geophysical Journal International* **102**, 695–731.

Taymaz, T., Jackson, J. & Mckenzie, D. 1991. Active tectonics of the north and central Aegean Sea. *Geophysical Journal International* **106**, 433–490.

Taymaz, T. & Price, S. 1992. The 1971 May 12 Burdur earthquake sequence, SW Turkey: a synthesis of seismological and geological observations. *Geophysical Journal International* **108**, 589–603.

Taymaz, T., Westaway, R. & Reilinger, R. 2004. Active faulting and crustal deformation in the Eastern Mediterranean region. *Special Issue of Tectonophysics*, **391**, Issues 1-4, 375 p., October 29, 2004, Elsevier Publications, Amsterdam, The Netherlands.

Taymaz, T., Yilmaz, Y. & Dilek, Y. 2007. The Geodynamics of the Aegean and Anatolia: Introduction. *In*: Taymaz, T., Yilmaz, Y. & Dilek, Y. (eds), *The Geodynamics of the Aegean and Anatolia*. The Geological Society, London, Special Publications **291**, 1–16.

Tavaloki, B. & Pezeshk, S. 2005. Empirical-stochastic ground-motion prediction for Eastern North America. *Bulletin Seismological Society of America* **95**, 2283–2296.

Theodulidis, N., Bard, P.Y., Archuleta, R. & Bouchon, M. 1996. Horizontal to vertical spectral ratio and geological conditions: the case of Garner Valley Down Hole array in Southern California. *Bulletin Seismological Society of America* **86**, 306–319.

Ulusay, R., Tuncay, E., Sönmez, H. & Gökçeoğlu, C. 2004. An attenuation relationship based on Turkish strong motion data and iso-acceleration map of Turkey. *Engineering Geology* **74**, 265–291.

Weisberg, S. 1980. *Applied Linear Regression*. Wiley, New York.

Westaway, R., Pringle, M., Yurtmen, S., Demir, T., Bringland, D., Rowbotham, G. & Maddy, D. 2004. Pliocene and Quaternary regional uplift in Western Turkey: the Gediz River terrace staircase and the volcanism at Kula. *Tectonophysics* **391**, 121–169.

Zare, M. & Bard, P.Y. 2002. Strong motion dataset of Turkey: data processing and site vlassification. *Soil Dynamics and Earthquake Engineering* **22**, 703–718.

Zhu, L., Akyol, N., Mitchell, B.J. & Sözbilir, H. 2006a. Seismotectonics of Western Turkey from high resolution earthquake relocations and moment tensor determinations. *Geophysical Research Letters* **33**, L07316, doi: 10.1029/2006GL025842.

Zhu, L., Mitchell, B.J., Akyol, N., Çemen, İ. & Kekovali, K. 2006b. Crustal thickness variations in the Aegean Region and its implications for the extension of continental crust. *Journal of Geophysical Research* **111**, B01301, doi:10.1029/2005JB003770.